Journal of Controlled Release 359 (2023) 116–131

Contents lists available at ScienceDirect

Journal of Controlled Release

journal homepage: www.elsevier.com/locate/jconrel

New-generation cytopharmaceuticals with powerfully boosted extravasation for enhanced cancer therapy

Luping Zhang [a,1], Qianqian Wang [a,1], Yupeng Dai [a], Jiaqi Chen [a], Tong Wu [a], Caoyun Ju [a], Lingjing Xue [a,*], Can Zhang [a,b,*]

[a] State Key Laboratory of Natural Medicines, Jiangsu Key Laboratory of Drug Discovery for Metabolic Diseases, Center of Advanced Pharmaceuticals and Biomaterials, China Pharmaceutical University, Nanjing 210009, China
[b] Chongqing Innovation Institute of China Pharmaceutical University, Chongqing 401135, China

ARTICLE INFO

Keywords:
Enhanced extravasation
Neutrophil cytopharmaceuticals
Cell membrane-anchoring strategy
Anti-angiogenesis
Chemotherapeutics

ABSTRACT

Effective extravasation of therapeutic agents into solid tumors still faces huge challenges. Since the doubted effectiveness of enhanced penetration and retention effect, first-generation neutrophil cytopharmaceuticals with encapsulated drugs have been developed to improve the drug accumulation in tumors based on the active chemotaxis and extravasation of neutrophils. Herein, a new generation of neutrophil cytopharmaceuticals with enhanced tumor-specific extravasation is reported to satisfy more complex clinical demands. This neutrophil cytopharmaceutical is obtained by anchoring vascular endothelial growth factor receptor 2 (VEGFR2)-targeting peptide K237 on neutrophil membrane after endocytosis of chemotherapeutics by neutrophils. Leveraging the cytokine-mediated active migration of neutrophils, the specific-recognition of K237 peptide to tumor vascular endothelium expedites the migration and enhances tight adhesion of neutrophils to vascular endothelium, thus improving the extravasation of therapeutic agents to target sites. Moreover, anti-angiogenesis effect from VEGFR2-blocking by K237 peptide achieves a cooperative tumor destruction with cytotoxic effects from released chemotherapeutics. This study demonstrates the great potential of enhanced proactive extravasation of cytopharmaceuticals via a cell-anchoring technology, leading to expedited drug infiltration and boosted therapeutic effects, which can be applied in other cell therapies to improve efficacy.

1. Introduction

Solid tumors are usually characterized by dense extracellular matrix, disorder vasculature [1], high interstitial fluid pressure [2], as well as hypoxia and faintly acid tumor microenvironment (TME) accompanying with immunosuppressive feature [3]. Despite great efforts have been put on the effective treatment of solid tumors, tumor cure still faces huge challenges. The primary reason can be ascribed to the inadequate contact between the therapeutic agents with target cells harbored by the TME. Notably, the limited extravasation of therapeutic agents from the circulation to the solid tumors acts as the first bottleneck of the inadequate contact, which determines the effective amounts of therapeutic agents within tumors [4,5]. It's understood that rapid blood clearance as well as the aberrant interstitial hypertension have been directly implicated in lower drug extravasation in tumor sites [6]. Thereby enhancing the extravasation to tumor is desirable to boost the drug accumulation and therapeutic efficacy.

Nanomedicine have been widely applied to improve the extravasation of therapeutic agents into tumor with attenuated systemic exposure based on the enhanced permeability and retention (EPR) effect [7]. To further exploit the extravasation potential of nanomedicine, nanocarriers modification involved in particle-size shrinking and ligand coupling for tumor-vasculature targeting have already been developed [8–12]. In parallel, increasing the permeability of the tumor vessels via external radiation and hyperthermia or lowering interstitial hypertension through anti-angiogenic treatment also contribute to the elevated extravasation of nanomedicine [6,13,14]. Despite that, the tremendous heterogeneity of tumor leaky vasculature among tumor types and even species has raised doubts about effectiveness of EPR as well as the extravasation efficacy of nanomedicine relying on EPR [15,16].

* Corresponding authors at: State Key Laboratory of Natural Medicines, Jiangsu Key Laboratory of Drug Discovery for Metabolic Diseases, Center of Advanced Pharmaceuticals and Biomaterials, China Pharmaceutical University, Nanjing 210009, China.
E-mail addresses: xuelingjing65@cpu.edu.cn (L. Xue), zhangcan@cpu.edu.cn (C. Zhang).
[1] These authors made equal contributions to this work.

https://doi.org/10.1016/j.jconrel.2023.05.037
Received 3 November 2022; Received in revised form 23 May 2023; Accepted 24 May 2023
Available online 7 June 2023

Additionally, external treatment such as radiation and hyperthermia for enhanced nanomedicine extravasation, which depend on specialized equipment and tumor types, also hamper the clinical accessibility. Thereby, spontaneous proactive extravasation to tumor indicates a more promising direction for cancer therapy.

Feasured as chronic inflammatory disease, solid tumors have established different chemokine gradients to recruit various leukocytes such as neutrophils, monocytes, lymphocytes, et al. [17]. The natural inflammation-tropism makes leukocytes hot vehicles candidates for anti-tumor therapy. Among them, neutrophils, the most abundant leukocytes in circulation, have attracted great attentions owing to their unique features, including earliest mobilization and proactive

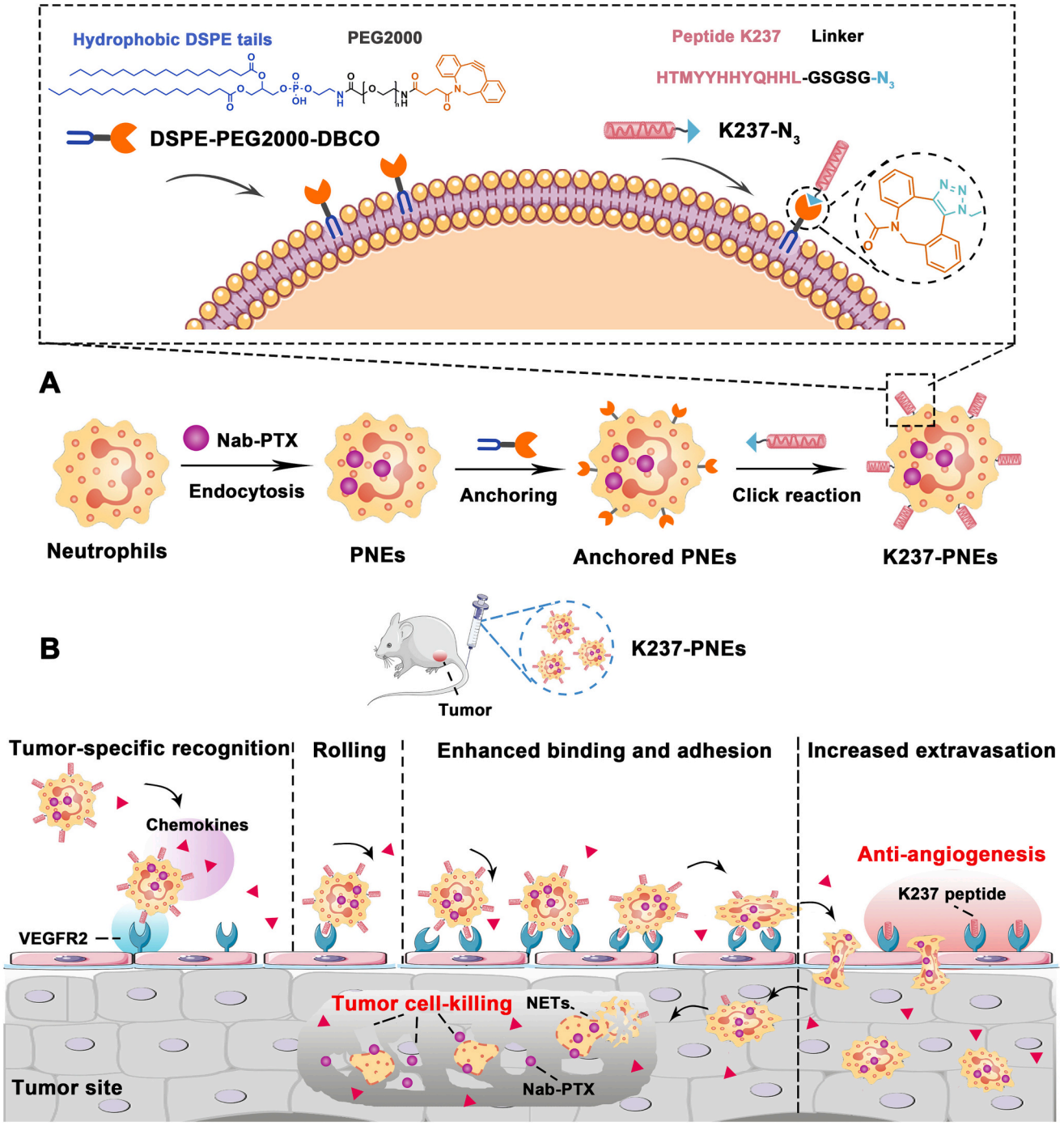

Fig. 1. Schematic illustration of K237-PNEs with enhanced tumor-specific extravasation achieving the combined antitumor effect. (A) Preparation of K237-PNEs. Neutrophil cytopharmaceuticals (PNEs) are firstly prepared via the endocytosis of nab-PTX as the traditional preparation technic, followed by the incubation with the anchoring molecules of DSPE-PEG2000-DBCO with a click group-dibenzocyclooctyne (DBCO). Next, azidation-K237 peptide (N_3-K237) is conjugated to the anchoring molecules through a facile click reaction between DBCO and azide group to gain the K237-PNEs. (B) After administration, K237-PNEs quickly response to the chemokines and migrate towards tumor inflammation sites. The highly-expressed PSGL-1, LFA-1, Mac-1, et al. on neutrophils as well as VEGFR2 recognization by anchored K237 peptide collectively initial the following rolling, binding and deformation of K237-PNEs. When extravasation from the blood to the tumor site, partial K237 peptide dislodge from the PNEs to inhibit the angiogenesis, while the infiltrated K237-PNEs can transport in the deep tissues and release the loading nab-PTX through the formation of NETs to kill tumor cells, thus achieving the combined efficacy against solid tumors.

extravasation into inflammation tissues [18]. Specifically, when sensing the gradient of chemokines, such as interleukin-8 (IL-8) [19], granulocyte colony-stimulating factor (G-CSF), and interleukin-17 (IL-17) [20,21], neutrophils will undergo tethering and rolling along the lining of the blood vessels, followed by firm adherence to endothelium through highly-expressed membrane chemokine receptors (CXCR1 and CXCR2), selectin ligands (PSGL1), and integrins (LFA-1 and Mac-1). Subsequently, neutrophils cross the endothelium and tissue barriers through the deformation, then extravasate into the inflamed sites [22,23]. Based on the inflammation-mediated chemotaxis of neutrophils, our group has fabricated the neutrophil cytopharmaceuticals with various nanomedicine loading to achieve highly enhanced drug deposition and superior therapeutic effects against solid tumors, with the help of adjuvant surgery, radiotherapy or photothermal therapy to provide enlarged inflamed cues [24–26]. Moreover, using the chemotaxis to some tumor-derived cytokines [27], the substantial suppression effect of neutrophil cytopharmaceuticals to tumor metastases has also been revealed [28–30].

Notably, neutrophils extravasation greatly relies on the strength of inflammation cytokines and the tight adhesion to vascular endothelium. The former determines the migration direction and targeting speed while the latter, as the initial step of extravasation, determines the transport speed and the site-specificity. More importantly, the tight adhesion of neutrophils to vascular endothelium mainly relies on the high-expression of integrins such as LFA-1 and Mac-1, which are closely regulated by local levels of inflammation cytokines in tumor microenvironment. Therefore, a more fundamental concern should be concentrated to increase the efficiency of tumor-specific targeting and extravasation of neutrophil cytopharmaceuticals, especially adapting to various levels of tumor inflammation. Significantly, tumor vascular endothelial cells also highly express some specific receptors such as vascular endothelial growth factor receptors (VEGFR) for triggering anomalous vascular hyperplasia [31,32]. This provides an opportunity by leveraging the recognition of VEGFR to tumor sites to promote targeting and further adhesion of neutrophils to vascular endothelium, thus facilitating the active extravasation of neutrophil cytopharmaceuticals. We conceive that the new generation of neutrophil cytopharmaceuticals with enhanced extravasation are more conducive to the clinical demands of tumor therapy.

Herein, we harnessed VEGFR2-targeting K237 peptide to modify the neutrophil cytopharmaceuticals for the dual therapeutic superiorities of enhanced neutrophils extravasation and angiogenesis suppression (Fig. 1). For triple-negative breast cancer (TNBC) with higher malignancy and metastatic potential, nanoparticle albumin-bound paclitaxel (nab-PTX) is a standard treatment but benefit only limited TNBC patients due to high tumor heterogeneity and lack of specific targets [33]. Owing to the active extravasation capacity of neutrophils, we have prepared the first-generation neutrophil cytopharmaceuticals with encapsulated nab-PTX (denoted as PNEs) to improve the nab-PTX infiltration and deposition within tumor sites where they can be release to take effect. While for VEGFR2-targeted peptide K237, it is better to be exposed outside the neutrophil cytopharmacruticals to recognize the binding sites during the circulation, thus enhancing neutrophil extravasation. Thus, we upgraded the drug-loading method from the first-generation based on endocytosis to the new-generation by anchoring K237 peptide on the membrane after endocytosis of nab-PTX, thus gaining nimble neutrophil cytopharmacuticals (K237-PNEs) [34]. K237-PNEs in vivo can migrate in respond to the tumor-released chemokines, which can meanwhile be accelerated by the recognition of K237 peptide to VEGFR2 on tumor vascular endothelium. This recognition subsequently facilitates K237-PNEs tight adhesion to the tumor-specific vascular sites, then initiates rolling and the following tumor-specific extravasation. Of note, K237 peptide serves as the anti-angiogenesis agents to promote tumor vascular normalization and reduce interstitial pressure for further enhanced neutrophils extravasation [35–37]. Extravasated K237-PNEs in tumor release the loaded nab-PTX to elicit tumor ablation and improve overall survival. In brief, the new-generation neutrophil cytopharmacuticals K237-PNEs, based on the improved drug-loading technics as well as the membrane-anchoring platform, have achieved the co-delivery of active peptide and chemotherapeutics. Moreover, the combined therapeutic efficacy of anti-tumor and anti-angiogenesis based on enhanced tumor-specific extravasation endow K237-PNEs with great clinical potential.

2. Materials and methods

2.1. Materials

Album-bound paclitaxel was purchased from Qilu Pharmaceutical Co., Ltd. (Jinan, China). K237 peptide (HTMYYHHYQHHL-GSGGS-N_3) and FITC-labeled K237 were purchased from Nanjing Peptide Biotechnology Co., Ltd. (Nanjing, China). DSPE-PEG2000-FITC, DSPE-PEG2000-DBCO and DSPE-mPEG2000 were purchased from Yare Biotechnology Co., Ltd. (Shanghai, China). Acetonitrile was purchased from TEDIA® (Anqing, China). Rhodamine B was purchased from Aladdin Biochemical Technology Co., Ltd. (Shanghai, China). APC anti-Ly6G, APC anti-CD62L, FITC anti-CD11b, Alexa Fluor 594 anti-CD31 and PE anti-CD16 were purchased from Biolegend (San Diego, CA, USA). Red Blood Cell Lysis Buffer, trypan blue and Hoechst 33342 were purchased from Beyotime Biotechnology Co., Ltd. (Shanghai, China). Percoll was purchased from GE Healthcare Co., Ltd.(Chicago, IL, USA). Annexin V-FITC/PI and Annexin V-PE/7ADD Apoptosis Detection Kit were all purchased from Vazyme Biotechnology Co., Ltd. (Nanjing, China). Cell Trace™ Far Red was purchased from Thermo Fisher Scientific (Waltham, MA, USA). VEGF was purchased from Abcam (Cambridge, UK). Anti-VEGFR2 antibody was purchased from Fine Biotech Co., Ltd. (Wuhan, China). 1,1-dioctadecyl-3,3,3,3-tetramethylindotricarbocyaine iodide (DiR) was purchased from KeyGEN Biotechnology Co., Ltd. (Nanjing, China). N-Formyl-Met-Leu-Phe (fMLP) was purchased from Sigma-Aldrich® (MA, USA). Matrigel was purchased from BD Biosciences (Bedford, MA, USA). Luciferase Cell Lysis Buffer was purchased from Thermo Fisher Scientific (Waltham, MA, USA).

2.2. Cell lines and animals

4 T1 mammary carcinoma cell lines and HUVECs cell lines were obtained from the Cell Bank of the Chinese Academy of Sciences. 4 T1 cell lines expressing luciferase (4 T1-Luci) were constructed by lab according to the manufacturer's protocol of lentivirus transfection of the firefly luciferase gene. 4 T1 and 4 T1-luci cell lines were incubated in 1640 medium (Gbico, CA, USA) and HUVEC were incubated in DMEM medium (Gbico, CA, USA). All culture system contained 10% FBS (Gbico, CA, USA) and 1% penicillin-streptomycin (Gbico, CA, USA) and the cells were cultured in a humidified incubator at 37 °C with 5% CO_2.

BALB/c mice (female, 6–8 weeks old, 18–20 g) were purchased from the Zhejiang academy of medical sciences. All animals were pathogen free and allowed access to food and water freely. All procedures were approved by the Animal Ethics Committee of China Pharmaceutical University and were conducted in compliance with the Guide for Care and Use of Laboratory Animals.

2.3. Preparation and characterization of PNEs

Rhodamine B-conjugated nab-PTX was prepared as follows. Album-bound paclitaxel (nab-PTX, 10 mg, 0.151 μmol) was dissolved in 500 μL PBS. Then 19.4 μL of Rhodamin B solution (5 mg/mL in water) was slowly added into the solution with stirring for 12 h in the dark at 25 °C. The reaction mixture was centrifuged at 12000 *g* for 10 min, followed by washing thrice with PBS. The Rhodamine B-conjugated nab-PTX was resuspended in water for further particle size and zeta potential measurement (Brookhaven Instruments Co., Ltd., NanoBrook Omni, USA).

Neutrophils were isolated from murine bone marrow according to a

modified method of our group. Briefly, the shanks and femurs isolated from normal mice were immersed in RPMI 1640 medium after removal of the muscle and sinew. Bone marrow was flushed from the bone with RPMI 1640, and centrifuged at 200 *g* (XIANGZHI Centrifuge, TDL5M, Changsha, China) for 3 min. The cell pellets were re-dispersed with 2 mL red blood cell lysis buffer and set at 4 °C for 3 min, followed by centrifugation at 200 *g* for 3 min (XIANGZHI Centrifuge). After re-dispersion in RPMI 1640, the unicellular suspension was added into a Percoll mixture solution, followed by centrifugation at 500 *g* for 30 min (XIANGZHI Centrifuge). The mature neutrophils were recovered at the interface of the 65% and 75% fractions and washed by ice-cold PBS thrice.

Fresh neutrophils (1×10^6 cells/mL) were resuspended with 5 mg/mL nab-PTX or Rhodamine B (Rho B) labeled nab-PTX in the mixture solution of saline and RPMI 1640 (1:3, *v/v*), where the final PTX concentration was 2 mg/mL, and incubated for 40 min at 37 °C. After washing with ice-cold PBS thrice, PNEs or Rho B-PNEs suspension were obtained and used immediately for the subsequent study. To quantify the amount of PTX in the PNEs, PNEs were disrupted by a cell lysis buffer. The cell lysate was collected and centrifuged at 10000 *g* for 5 min (Beckman Coulter Inc., Allegra 64R Benchtop Centrifuge, USA). The 50 μL supernatant was mixed with 200 μL of acetonitrile, vortexed for 5 min and centrifuged at 10000 *g* for 10 min (Beckman). After that, 20 μL supernatant was injected into the HPLC system (SHIMADZU Co., Ltd., LC-2010A, Japan) for further analysis. Rho B-PNEs were observed by confocal laser scanning microscope (CLSM; Carl Zeiss Co. Ltd., LSM800, Germany). Annexin V-FITC/PI Apoptosis Detection Kit was used to investigate the effect of incubation process on cell viability by flow cytometry (Thermo Fisher Scientific, Attune NXT, USA).

2.4. Preparation and characterization of lipid-anchored PNEs

The membrane-anchored PNEs were prepared as follows. Rho B-PNEs were firstly incubated with 50 μM DSPE-PEG2000-FITC for 10 min in culture medium containing 20 μL PEG400, then centrifuged to collect the cells. On the other side, neutrophils were firstly incubated with 50 μM DSPE-PEG2000-FITC for 10 min in the same conditions, then incubated with Rho B-conjugated nab-PTX as mentioned above. The membrane-anchoring effect were respectively observed by CLSM to determine the order of the cell modifications.

To investigate the optimal anchoring concentration and incubation time of DSPE-PEG2000-FITC, PNEs firstly were incubated with different concentrations of DSPE-PEG2000-FITC for 10 min in the culture medium mentioned above to gain the optimal anchoring concentration. Then PNEs were incubated with DSPE-PEG2000-FITC for different time at the optimal concentration above to gain the optimal incubation time. The membrane anchoring effect was evaluated by flow cytometry (Thermo) and CLSM (Zeiss). To further confirm the anchoring position at membrane, anchored PNEs were labeled with APC anti-Ly6G antibody on the cell membrane. The fluorescence co-localization was observed and analyzed by CLSM (Zeiss). The cell viability of incubation process was investigated by Annexin V-PE/7-AAD Apoptosis Detection Kit as described above.

2.5. Quantitatively analysis of DSPE-PEG2000-FITC anchored on PNEs

The method of trypan blue (TB) quenching was here used to investigate the proportion and amount of membrane-anchored DSPE-PEG2000-FITC on the whole cell. DSPE-PEG2000-FITC anchored PNEs were incubated with TB solution of differnent concentrations. The optimal concentration of TB solution corresponds to the unchanged fluorescence intensity, meaning the FITC fluorescence on NEs membrane is totally quenched and with no damage to membrane integrity, as determined by flow cytometry and Annexin V-PE/7-AAD Apoptosis Detection Kit. Then the proportion of membrane-anchored DSPE-PEG2000-FITC was calculated with the following Eq. (1):

$$\text{Membrane anchoring}\ (\%) = (\mathrm{MFI_b} - \mathrm{MFI_a})/\mathrm{MFI_b} \times 100\% \quad (1)$$

Here $\mathrm{MFI_a}$ and $\mathrm{MFI_b}$ represented the mean fluorescence intensity of PNEs (10,000 events) by flow cytometry (Thermo) after and before TB quenching.

To investigate the anchoring amount of DSPE-PEG2000-FITC on membrane, the incubation supernatant after membrane anchoring was collected. The fluorescence intensity of the initial added anchoring molecules and the incubation supernatant were respectively measured at excitation and emission wavelengths of 495 nm and 520 nm by microplate reader (BioTek Instruments, Inc., Synergy H1, USA). The fluorescence intensity was converted into the concentration of DSPE-PEG2000-FITC through the standard curve of serial dilutions of stock solution, then the concentration multiplied by the volume made the mol amount of DSPE-PEG2000-FITC. The amount of DSPE-PEG2000-FITC on membrane per 10^6 cells was obtained by the following Eq. (2):

$$\text{Anchoring amount} = (\mathrm{m_i} - \mathrm{m_s}) \times \text{membrane anchoring}(\%) \quad (2)$$

Here $\mathrm{m_i}$ and $\mathrm{m_s}$ were respectively the molar quantity of the initial anchoring molecules and the incubation supernatant. After several time of washing, the supernatant of each time was collected to analyze the washing loss of the anchored molecules on membrane as mentioned above.

The in vitro membrane-anchoring stability of PNEs was investigated in RPMI 1640. The distribution change of DSPE-PEG2000-FITC on NEs was analyzed by the MFI of whole cells before and after trypan blue quenching at different time based on the calculation methods above. And the supernatant after incubation of different time were also collected for fluorescence intensity detection by the microplate reader (BioTek). The fluorescence change of anchored cells at different time were observed by CLSM (Zeiss).

2.6. Preparation and characterization of K237-PNEs

Briefly, DSPE-PEG2000-DBCO anchored PNEs were firstly incubated with series of concentrations of FITC-N_3-K237 for 1 h in RPMI 1640 medium. After confirming the optimal concentration, the anchored PNEs incubated with FITC-N_3-K237 for different time to determine the most suitable incubation time. The cell viability of incubation process was investigated by Annexin V-PE/7-AAD Apoptosis Detection Kit. Blank PNEs were set as the control to reveal the anchoring of K237 peptide by biological orthogonal reactions rather than passive adsorption. Besides, to confirm the distribution of anchored K237 on cell membrane, K237-PNEs were labeled with APC anti-Ly6G antibody and stained with Hoechst 33342, followed by observation and analysis of the fluorescence colocalization by CLSM (Zeiss).

The method of TB quenching was also used to detect the proportion of K237-anchored on membrane in the whole cell. The optimal TB concentration as well as the proportion of membrane-anchored K237 peptide was determined as described above. The amount of anchored K237 peptide on neutrophil membrane were also calculated in line with the above methods.

2.7. Evaluation of physiological functions of K237-PNEs

The chemotaxis of K237-PNEs was investigated using a transwell migration assay (polycarbonate membrane: 3 μm pore size, 12 mm diameter and 1.12 cm^2 membrane surface area, Corning). Beforehand the supernatant of 4 T1 cells cultured for 24 h was collected as tumor conditioned medium (TCM). Then K237-PNEs and blank neutrophils (1×10^6 cells/mL) were seeded into the upper transwell chamber, and RPMI 1640 containing 10% FBS (*v/v*) with 0% TCM, 10% TCM, 50% TCM and 100% TCM respectively were added in the lower chamber. After 3 h of incubation, the number of neutrophils in the lower chamber was counted. The chemotaxis index was calculated from the following

Eq. (3):

$$\text{Chemotaxis index} = (N_{TCM} - N_{control})/N_{control} \quad (3)$$

N_{TCM} was the counted numbers of neutrophils in the lower chamber after incubating with each formulation in the presence of TCM, and $N_{control}$ was the number of blank neutrophils in the lower chamber without TCM.

To evaluate the transvascular migration capacity of K237-PNEs, we constructed a blood vessel model with HUVEC monolayer in the transwell cell culture system (Corning). Briefly, HUVEC (1×10^5 cells) were seeded into the upper transwell chamber, and cultured in the medium DMEM containing 10% FBS in the lower chamber. The integrity of the cell monolayer was evaluated by measuring the TEER values using a Millicell-ERS voltohmmeter (Millipore Corporation, Millicell® ERS-2, MA, USA), which above 300 $\Omega \cdot cm^2$ suggested the blood vessel model was successfully constructed. Then, K237-PNEs and blank neutrophils (1×10^6 cells/mL) were added into the upper chamber, and RPMI 1640 containing 10% FBS (*v/v*) with 0% TCM, 50% TCM and 100% TCM respectively were added into the lower chamber. After 8 h of incubation, the number of neutrophils in the lower chamber was counted.

The expression of several critical membrane biomarkers such as CD11b, CD62L, and CD16 were respectively detected with flow cytometry (Thermo). Blank neutrophils were used as control. The membrane-impermeable dye 7AAD was used for detecting the impact of anchoring process on membrane integrity and the dead neutrophils were used as the 7ADD positive group.

2.8. Anchoring stability and drug release of K237-PNEs in different physiological conditions

The stability in K237-PNEs under normal physiological conditions was evaluated by incubating K237-PNEs (1×10^6 cells/mL) in RPMI 1640 for different periods (0, 1, 2, 4, 6, and 8 h). The PTX amount in the cytosol and released to the supernatant were determined using HPLC (SHIMADZU) respectively.

The release of PTX and K237 from K237-PNEs during chemotaxis and transvascular migration were investigated with a transwell culture system (polycarbonate membrane: 3 μm pore size, 24 mm diameter and 4.67 cm^2 membrane surface area, Corning). During chemotaxis, K237-PNEs (1×10^6 cells/mL) were seeded into the upper transwell chamber and incubated in RPMI 1640 containing 10 nmol/L fMLP in the lower chamber for different time. The amount of PTX in the K237-PNEs and released to the supernatant were determined using HPLC (SHIMADZU). The amount of K237 anchored on membrane was measured using microplate reader (BioTek) by the method trypan blue quenching, and meanwhile the amount of K237 released to the supernatant was collected for fluorescence intensity detection by the microplate reader (BioTek). In the case of transvascular migration, K237-PNEs (1×10^6 cells/mL) were seeded into the upper chamber of the blood vessel model constructed with HUVEC monolayer mentioned above, and incubated in RPMI 1640 containing 10 nmol/L fMLP in the lower chamber for 8 h. Collected K237-PNEs from the lower chamber were counted and then measured for fluorescence intensity using microplate reader (BioTek). To investigate the binding of K237 peptide to the membrane receptor VEGFR2, the HUVEC seeded on the polycarbonate membrane of a transwell chamber were gently digested and collected for cell counting, then quantified for fluorescence intensity with microplate reader (BioTek) and imaged with CLSM (Zeiss).

To investigate the PTX release through NET formation induced by inflammation, K237-PNEs (1×10^6 cells/mL) were incubated in 100% TCM medium simulating the tumor inflammation environment. After 12 h of incubation, the cells were washed with cold PBS and fixed in 4% PFA. The fixed cells were then labeled with APC anti-Ly6G and stained with Hoechst 33342, followed by observation by CLSM (Zeiss).

2.9. In vitro anti-angiogenesis and tumor-killing effect of K237-PNEs

To investigate the effect of cyto-pharmaceuticals on the proliferation of vascular endothelial cell, Cell Trace™ Far Red labeled HUVEC were seeded on 24-well plate (1×10^5 cells per well). Different formulations were added subsequently, including nab-PTX (5 μg/mL), K237 peptide (5.8 nmol/mL), K237 peptide (5.8 nmol/mL) combined with nab-PTX (5 μg/mL), blank NEs (2×10^6 cells/mL), as well as K237-PNEs (2×10^6 cells/mL). The fresh medium of DMEM medium with 10% FBS was used as a negative control. After 48 h of incubation, the supernatant was removed and the HUVEC were collected through tryptase digestion followed by detection via flow cytometry (Thermo).

To evaluate the effect of K237-PNEs on the migration of vascular endothelial cell, a transwell assay (polycarbonate membrane: 8 μm pore size, 24 mm diameter, Corning) was used for the following test. HUVEC (2×10^5 cells/mL) were seeded into the upper chamber and VEGF (20 ng/mL) in DMEM complete medium was added in the lower chamber to stimulate the migration of HUVEC. Different medium or formulations were added into the upper chamber including: 1) nab-PTX (5 μg/mL) 2) K237 peptide (5.8 nmol/mL) 3) K237 peptide (5.8 nmol/mL) and nab-PTX (5 μg/mL) 4) blank NEs (2×10^6 cells/mL) 5) K237-PNEs (2×10^6 cells/mL). The fresh DMEM complete medium in the lower chamber was used as a negative control. After 12 h of incubation, the cells in the lower chamber were counted. The inhibition ratio was calculated by the following Eq. (4):

$$\text{Inhibition ratio}(\%) = 1 - (N_s - N_n)/(N_p - N_n) \times 100\% \quad (4)$$

Here N_p and N_n represented the counted number of the group treated with 20 ng/mL VEGF and DMEM complete medium, respectively, while N_s represented the counted number of the other groups.

To investigate the anti-angiogenesis effect, the matrigel dissolved at 4 °C in advance was laid in 8-well plate (ibidi, Germany). Then, the 8-well plate was placed at 37 °C until the matrigel fully solidified. After that, 50 μL of cell suspension (2×10^4 HUVEC cells) was added to each well and scratches or glue damage should be avoided in the meantime. Subsequently, 50 μL of different medium or formulations were added, including VEGF (20 ng/mL), blank NEs (1×10^5 cells), nab-PTX (0.25 μg), PNEs (1×10^5 cells), K237 + nab-PTX (0.29 nmol+0.25 μg), K237 (0.29 nmol), and K237-PNEs (1×10^5 cells). The fresh medium of DMEM medium was used as a negative control. After 6 h of incubation, the angiogenesis was observed by inverted microscope. The branches points and length of neovascularization were analyzed by image J.

To further evaluate the in vitro tumor-killing effect, 4 T1-Luci cells (1×10^5 cells per well) were seeded on a 24-well plate and treated with different formulations including nab-PTX (5 μg/mL), K237 peptide (5.8 nmol/mL), K237 peptide (5.8 nmol/mL) combined with nab-PTX(5 μg/mL), blank NEs (2×10^6 cells/mL), and K237-PNEs (2×10^6 cells/mL) for 12 h. The fresh medium of 1640 medium with 10% FBS was used as a control. After washing with cold PBS twice, the cells were treated with the luciferase reporter cell lysis buffer and incubated for 15 min on ice. After centrifugation at 12000 rpm (Beckman) for 4 min, the supernatant (20 μL) was mixed with Luciferase Assay Kit (100 μL) in a 96-well black plate and incubated for 5 min, followed by detection via microplate reader (BioTek).

2.10. Neutrophils extravasation in vivo

To establish an orthotopic triple negative breast cancer model, 4 T1 cells (2×10^6 cells) suspended in 100 μL PBS were injected into the right mammary fat pad of female BALB/c mice (6–8 weeks). The tumor volume was monitored every day until up to 100 cm^3. The tumor tissues were isolated to prepare the frozen tissue sections. The sections were labeled with Alexa Fluor 594 anti-CD31 antibody and anti-VEGFR2 antibody with Alexa Fluor 488 goat anti-rabbit IgG to evaluate the VEGFR2 expression on tumor vessels by CLSM (Zeiss). The mammary fat

pad of normal mouse was treated as the control.

After that, 4 T1 tumor-bearing mice (3 mice per group) were intravenously injected with DiR-labeled NEs, PNEs and K237-PNEs (2×10^7 cells). The mice were imaged at different time points of post-injection (4, 12, 24 and 48 h) using in vivo imaging system (PerkinElmer Inc., IVIS® Spectrum, MA, USA). Meanwhile, the tumor tissues and other organs (liver, spleen, heart, lung and kidney) were also harvested and imaged. The total radiant efficiency of region-of-interest (ROI) in mice and isolated tumor tissues were respectively analyzed by IVIS spectrum. The frozen tumor tissue sections were prepared to observe the distribution of DiR-labeled different neutrophils cytopharmaceuticals using CLSM (Zeiss).

For observing the migration and extravasation from blood vessels for neutrophils, real-time intravital observation were carried out on the 4 T1 tumor-bearing mice through FVMPE-RS system (Olympus). When the tumor reached a size of 100 mm^3, the mice were intravenously injected PNEs and K237-PNEs (2×10^7 cells) in which neutrophils, nab-PTX and K237 were respectively labeled by Cell Trace Far Red, Rhodamine B and FITC. After 1 h of neutrophils injection, mouse was under anaesthetic by intraperitoneal injection of 200 μL chloral hydrate (40 mg/mL). On the premise of not destroying the peritoneum, the epidermis of the tumor site in mouse was carefully removed by separating epidermis from the peritoneal wall with forceps until fully exposing the tumor tissue and the surface microvessels. The mouse was then placed on a thermoplate and the blood vessels were held in place through a rounded vacuum chuck equipped on the FVMPE-RS system. Saline was dripped onto the surface of rounded vacuum chuck then the microscope lens (25×/1.05 water immersion objective, numerical aperture = 1.05) was placed close to the vacuum chuck to observe the vessels. During the process, sterile saline solution (37 °C) was dripped on the exposed peritoneum of mouse to keep the local moisture. Multiple fields were randomly selected for observation and imaging was performed continuously for 10–20 min with acquisition rate 20–25 frames/min. The imaging results were processed with OLYMPUS FV31S-SW. Then the tumor tissues were isolated at different time points after neutrophils injection (1, 2, 4 and 8 h) and the frozen tumor sections were prepared then labeled with Alexa Fluor 594 anti-CD31 antibody to indicate the tumor blood vessels. The process of vessels-binding and extravasation of different neutrophils cytopharmaceuticals labeled by DiR were observed by CLSM (Zeiss).

The biodistribution of PTX and K237 were also quantitatively detected in tumors and normal organs, which can also demonstrate the tumor-targeting and extravasation effect of different neutrophils cytopharmaceuticals. Briefly, 4 T1 tumor-bearing mice were intravenously injected with nab-PTX + K237 (2.5 mg/kg PTX and 2.9 μmol/kg K237), PNEs (1×10^9 cells/kg, equivalent to 2.5 mg/kg PTX) and K237-PNEs (1×10^9 cells/kg, equivalent to 2.5 mg/kg PTX and 2.9 μmol/kg K237) and sacrificed at different time points of post-injection (4, 12, 24 and 48 h) to harvest the tumors tissues and other normal organs. All tissues were weighted and then homogenized in saline. The homogenate was mixed with acetonitrile of the same volume, vortexed for 5 min and centrifuged at 10,000 *g* (Beckman) for 10 min to collect the supernatant. The fluorescence intensity of K237 and the amount of PTX from the supernatant were directly detected with microplate reader (BioTek) and HPLC (SHIMADZU), respectively.

2.11. In vivo antitumor effect and safety evaluation

4 T1 tumor-bearing mice were divided to five groups receiving saline, nab-PTX (2.5 mg/kg), K237 (2.9 μmol/kg), NEs (1×10^9 cells/kg), K237 + PNEs (2.9 μmol/kg K237, 1×10^9 cells/kg PNEs equivalent to 2.5 mg/kg PTX), and K237-PNEs (1×10^9 cells/kg, equivalent to 2.5 mg/kg PTX and 2.9 μmol/kg K237) every two days. The body weights and tumor volumes were monitored every two days during treatment. At Day 25, the mice were sacrificed to harvest the blood samples, tumor tissues and normal organ tissues, and recorded the weights of all tumor and tissue samples. The paraffin sections of tumor tissues were stained with H&E for tumor proliferation observation and the frozen sections of tumor tissues were used to evaluate the anti-angiogenesis effect by immunofluorescence detection. The survival was monitored every day until all mice died. All mice required humane sacrifice if tumor size exceeded 15 mm in diameter.

The harvested blood samples of the mice were used for safety evaluation such as blood routine examination and biofunction evaluation of liver and kidney, including alanine transaminase, aspartate transaminase, alkaline phosphatase, lactic dehydrogenase, and urea nitrogen. Besides, for pathology research, paraffin sections of the normal organs was stained with H&E and visualized by inverted fluorescence microscope (Olympus, Japan). The organ index was also calculated from the ratio of organs weight/body weight.

2.12. Statistical analysis

Statistical analyses were performed using the GraphPad Prism 8.0 software. All graphical data were presented as mean ± SEM in at least triplicate. Statistical significance was determined using two-tailed Student's *t*-test for or One-way ANOVA, in which P values <0.05 were considered statistically significance. A log-rank (Mantel-Cox) test was used to analyze the statistical significance in the survival analysis.

3. Results

3.1. Characterization of lipid-anchored neutrophils

Although membrane-anchoring has been performed in the non-phagocytes T cells in our previous report [38], the anchoring strategy whether could work on the typical phagocytes neutrophils remains unclear. Herein, we first optimized the membrane-anchoring methods of the anchoring lipid (DSPE-PEG2000-DBCO) for neutrophils and DSPE-PEG2000-FITC was used for convenient monitoring. After incubation with 50 μM DSPE-PEG2000-FITC in culture medium, an effective fluorescence co-localization between APC anti-Ly6G, a specific membrane biomarker of neutrophils, and DSPE-PEG2000-FITC was observed by confocal laser scanning microscopy (CLSM), which indicated the successful membrane-insertion with nearly invisible uptake in the cytosol (Fig. 2A and B).

Since K237-PNEs involves the process of the endocytosis of nab-PTX and the K237 peptide anchoring on membrane, the construction sequence plays vital roles in the drug loading and stability of K237-PNEs. Thus, we prepared rhodamine-labeled nab-PTX (similar particle size and zeta potential with nab-PTX, Supporting Information Fig. S1A) for observing and comparing separate loading sequences. Firstly, we prepared PNEs according to our first-generation preparation technics, which held the drug loading of PTX about 2.5 μg PTX per 10^6 cells and unchanged viability with fresh neutrophils (Supporting Information Fig. S1B). Moreover, the rhodamine-labeled nab-PTX distributed uniformly in the cytosol of neutrophils, indicating an effective cellular uptake (Supporting Information Fig. S1C). Next, similar membrane-anchoring effect was reproduced when PNEs incubated with anchoring lipid under the same condition (Supporting Information Fig. S2A). In contrast, on condition that neutrophils underwent membrane-anchoring followed by the endocytosis of nab-PTX, strong FITC fluorescence in the cytoplasm was observed and colocalized with the RhoB-labeled nab-PTX, suggesting this loading process caused decreased anchoring stability (Supporting Information Fig. S2B). In consequence, membrane anchoring after the nab-PTX endocytosis indicated a better sequence to maintain a higher anchoring efficacy.

Next, we optimized the incubation conditions of DSPE-PEG2000-FITC to achieve the optimal anchoring effect with minimum endocytosis and cell apoptosis. Although no obvious cell cytotoxicity was detected after incubation with DSPE-PEG2000-FITC at the concentration from 5 μM to 100 μM for 10 min, the noticeable cellular uptake of anchoring molecules at the concentration above 50 μM was observed

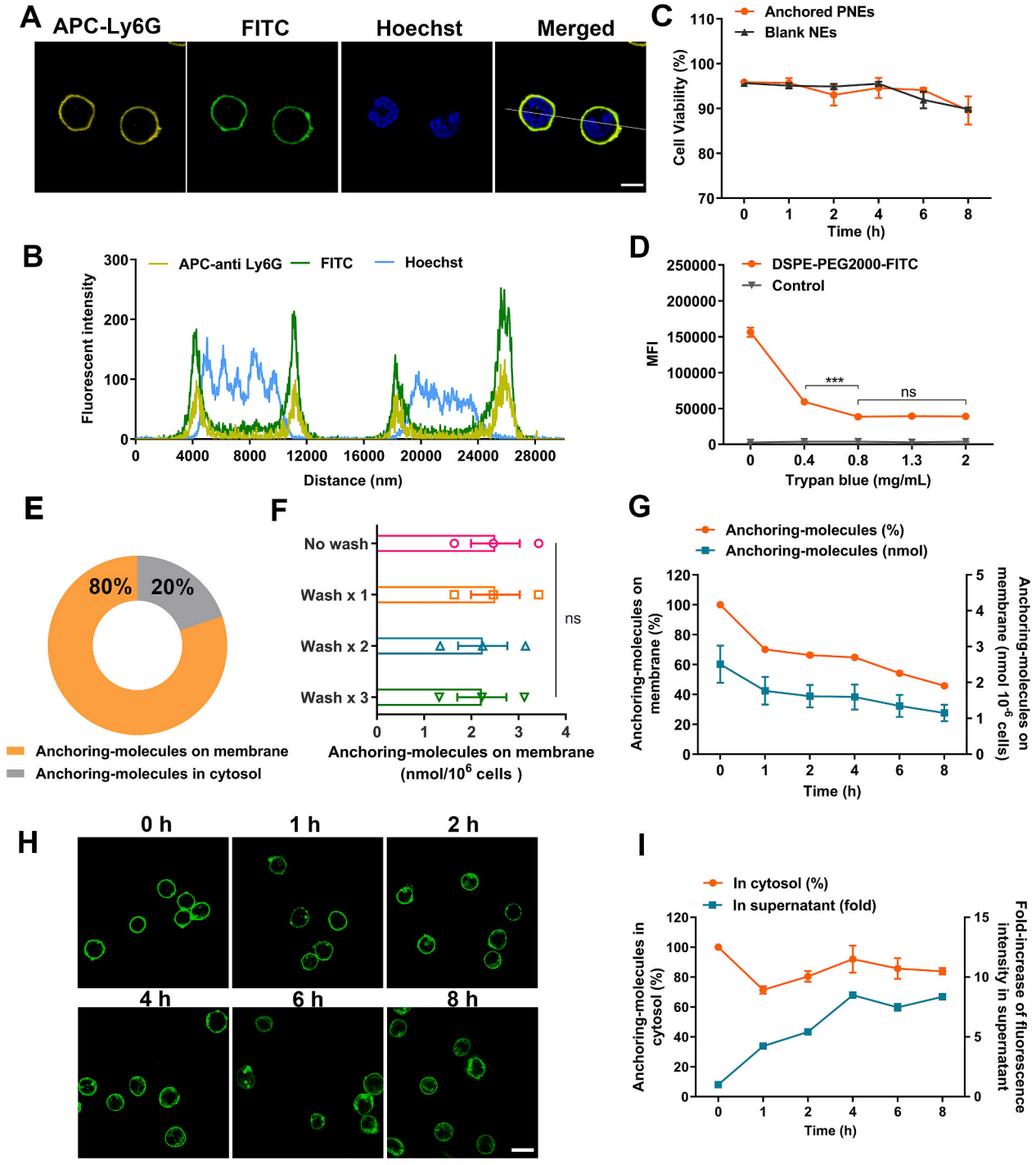

Fig. 2. Characterization of lipid-anchored neutrophils. (A) The fluorescence co-localization and (B) quantitative fluorescence intensity of anchoring molecules (DSPE-PEG2000-FITC) and APC anti-Ly6G labeled cell membrane. Scale bar = 5 μm. Images are representative of 2 independent experiments. (C) Cell viability of anchored PNEs in RPMI 1640 within 8 h, compared with blank NEs. (D) The optimal trypan blue-quenching concentration was determined by the related mean fluorescence intensity (MFI) reduced to a constant value. Blank NEs set as the control. (E) The ultimate ratio of anchoring molecules on cell membrane and in the cytosol. (F) The quantification of anchoring molecules on membrane per 10^6 NEs after repeated washing. (G) The stability of anchoring molecules on membrane within 8 h. The percentage and the specific amount of retained anchoring molecules on membrane were showed in red dots and blue boxes respectively. (H) The stability of anchoring molecules on membrane observed by CLSM in real time. Scale bar = 10 μm. (I) Quantification of the distribution of DSPE-PEG2000-FITC in NEs cytosol and incubation supernatant over time. All data are mean ± SEM ($n = 3$). ***$P < 0.001$. ns, not significant. (For interpretation of the references to colour in this figure legend, the reader is referred to the web version of this article.)

(Supporting Information Fig. S3). With the fixed 50 μM of DSPE-PEG2000-FITC, the cellular uptake increased while the cell viability decreased as time extended (Supporting Information Fig. S4). Based on comprehensive consideration, a transient incubation of PNEs with DSPE-PEG2000-FITC (50 μM) for 10 mins achieved the optimal anchoring effect with limited adverse impact. Moreover, membrane-anchored PNEs showed nearly the same cell viability for up to 8 h in vitro compared with blank neutrophils (Fig. 2C). To further quantify the proportion of anchoring molecules both on the membrane and in the cytoplasm, trypan blue (TB) quenching (0.8 mg/mL, Fig. 2D and

Supporting Information Fig. S5) was applied to quench the FITC fluorescence on the membrane without interference to those in cytoplasm [39–41]. Calculated by this, about 80% of anchoring molecules (equivalent to 2.5 nmol per 10^6 cells) was distributed on the membrane through the hydrophobic insertion even after washing for 3 times (Fig. 2E and F), while the left entered the cytoplasm by cell endocytosis.

In view of the active endocytosis and secretion of neutrophils, the stability of membrane-anchored molecules set up a vital basis for the subsequent applications. The proportion of membrane-anchored molecules over time was also quantified through TB quenching. We found

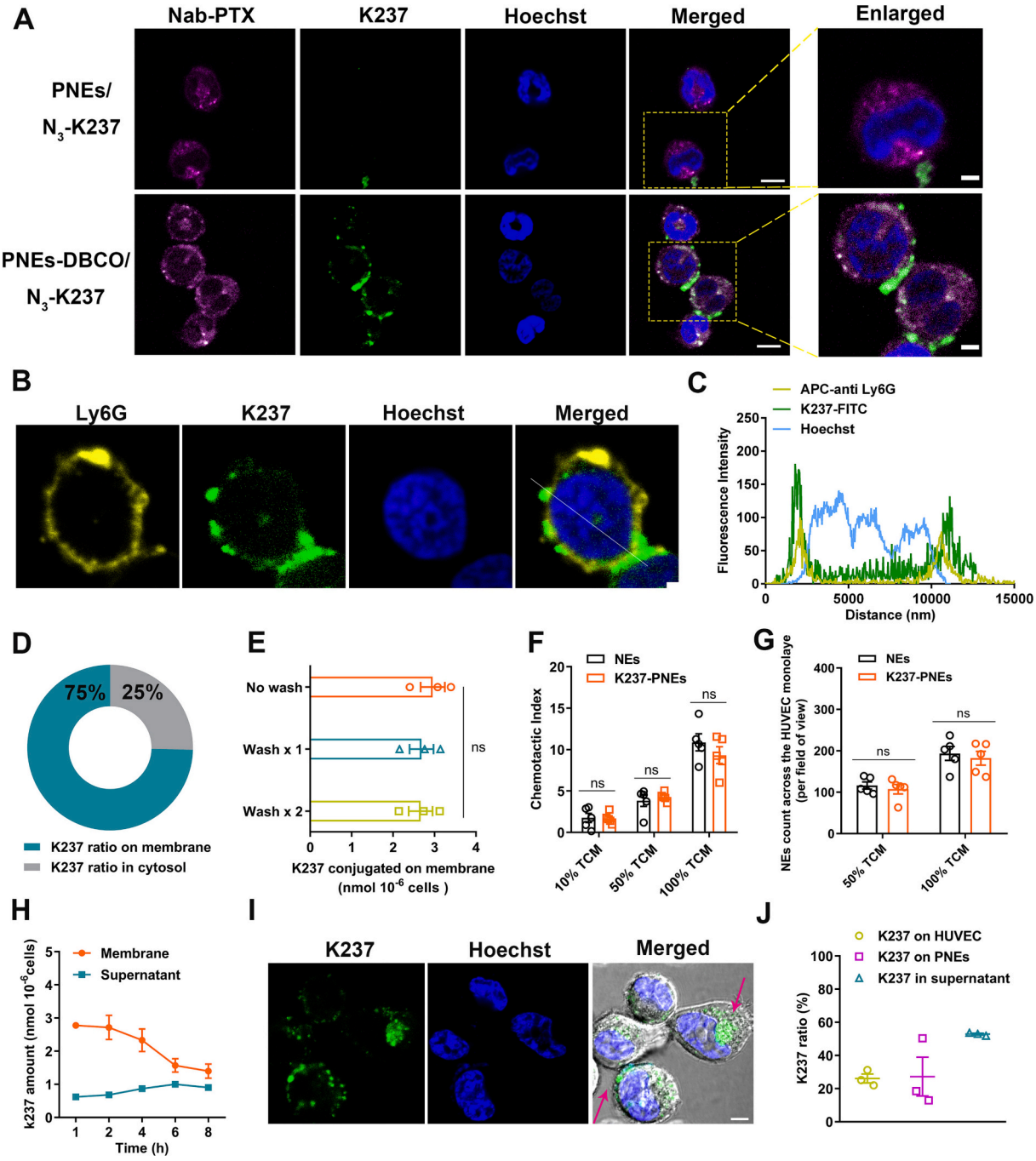

Fig. 3. Preparation and characterization of K237-PNEs. (A) The confocal images of K237-anchored PNEs on neutrophils by incubating N_3-K237 (100 μM) with DBCO-anchored PNEs for 1 h. PNEs anchored with DSPE-mPEG2000 treated in the same way set as a control. Scale bar was 5 μm in the merged images and 2 μm in the enlarged view. Images are representative of 3 independent experiments. (B) The fluorescence distribution and co-localization of conjugated K237 peptide with APC anti-Ly6G labeled membrane. Scale bar = 2 μm. (C) The related fluorescence quantitative results along the white line in B. (D) The ultimate ratio of K237 peptide on cell membrane and in the cytosol. Data are representative of 2 independent experiments. (E) The quantification of K237 conjugated on the membrane per 10^6 NEs along with repeated washing. Data are mean ± SEM ($n = 3$). (F) The chemotactic index of K237-PNEs and blank NEs. Data are mean ± SEM ($n = 5$ random view). (G) The average NEs counts through transendothelial migration to the lower chamber, calculated from five random fields of view. Data are mean ± SEM (n = 5). (H) Determination of the quantity of anchored K237 peptide dislodged from K237-PNEs during the chemotaxis migration for 8 h. Data are mean ± SEM (n = 3). (I) The binding of dislodged K237 peptide with HUVEC during the transendothelial migration assay, as observed by CLSM and indicated by magenta arrows. Scale bar = 5 μm. (J) Quantification of the distribution of K237 peptide during transendothelial migration assay. Data are mean ± SEM (n = 3). ns, not significant. (For interpretation of the references to colour in this figure legend, the reader is referred to the web version of this article.)

about 75% of initial anchored molecules, equivalent to 1.62 nmol per 10^6 cells, remained anchoring on the membrane within 2 h of incubation at 37 °C. However, the membrane proportion reduced to 50%, about 1.25 nmol per 10^6 cells, after 8 h of incubation (Fig. 2G). Notable attenuation of membrane fluorescence with time was also observed by CLSM in consistent with the fluorescence quantification (Fig. 2H). Therefore, the subsequent K237 conjugation should be finished within 2 h to ensure the maximum K237-coupling efficiency. To further investigate the reason of reduced anchoring molecules, the amounts of molecules in the cytoplasm and incubation supernatant were measured respectively. The intracellular fluorescence change of membrane-anchored molecules was less evident than that in supernatant with time (Fig. 2H and I), which indicated that shedding off from the membrane rather than cell internalization was the main reason. It was worth noting that most physiological functions of neutrophils depended on the rapid membrane lipid fluidity, which exacerbated the tendency towards shedding off from membrane than energy-consuming endocytosis, exerting an unfavorable impact on the stability of anchored molecules. Taken together, these results indicated a relatively stable and highly efficient membrane-anchoring technique for PNEs being established.

3.2. Preparation and characterization of K237-anchored neutrophil cytopharmaceuticals

To maximize the conjugation efficiency of K237 peptide to DSPE-PEG2000-DBCO on PNEs, we first optimized the bio-orthogonal reaction conditions between PNEs and N_3-K237 peptide labeled with FITC for visualization. Although the ratio of fluorescent PNEs elevated to 89% as the concentration of N_3-K237 peptide rose to 200 μM (Supporting Information Fig. S6A—C), the endocytosis of N_3-K237 peptide by PNEs was obviously observed by CLSM when the concentration higher than 100 μM (Supporting Information Fig. S7A). It implied that higher K237 concentration might lead to more cellular internalization, thus 100 μM of N_3-K237 peptide was applied in the following studies. Besides, we found that the extended incubation time of 1 h improved the coupling of N_3-K237 peptide to DSPE-PEG2000-DBCO with a positive ratio of about 77% (Supporting Information Fig. S7B and Fig. S8). More importantly, the conjugation process had been demonstrated friendly to cell viability (Supporting Information Fig. S6D and Fig. S8D). As shown in Fig. 3A and Fig. S9A (Supporting Information), the fabricated K237-anchored neutrophil cytopharmaceuticals presented a cluster or strip state of fluorescence of K237 peptide on neutrophil membrane and uniformly dispersed fluorescence of RhoB-labeled nab-PTX in cytosol. In contrast, there was limited fluorescence of K237 peptide on PNEs without the anchoring of DSPE-PEG2000-DBCO. The location of K237 peptide was further confirmed on the neutrophil surface by the fluorescent overlap between neutrophil membrane labeled by APC anti-Ly6G and the anchored K237 peptide (Fig. 3B and C). Similarly, nearly 75% of K237 peptide (equal to 2.9 nmol per 10^6 cells) anchoring on the cell surface was calculated by the TB quenching method (Fig. 3D, Supporting Information Fig. S9B and S9C). However, there was only 2.5 nmol of DSPE-PEG2000-DBCO anchored on neutrophil membrane as mentioned in Fig. 2E. The mainly reason can be ascribed to the physical absorption of K237 peptide to the membrane, which was further confirmed by the decreased amount of K237 peptide by 10% after a single washing but without further decrease after repeated washing (Fig. 3E). These results suggested that nearly 100% of DSPE-PEG2000-DBCO on the surface being conjugated with N_3-K237 with high efficiency.

In addition, the physiological functions of neutrophils after sequential manufactures should be take into consideration, which determines the in vivo fate of the K237-anchored neutrophil cytopharmaceuticals. Firstly, we explored the membrane integrity through a fluorescent dye, 7-aminoactinomycin D (7-AAD), which cannot transport across the intact cell membrane. The complete destroy of membrane integrity for dead cells meant around 98% 7-ADD staining, and the DSPE-PEG2000-DBCO anchoring and the subsequent K237 conjugation caused minimal influx of 7-AAD than dead cells (Supporting Information Fig. S10A and B), indicating the retained membrane integrity of modified neutrophils. Moreover, the expressions of critical membrane markers (CD11b, CD62L, CD16) associated with cell adhesion and migration was little affected compared with blank NEs (Supporting Information Fig. S10C), suggesting the vital neutrophils membrane proteins were not blocked by K237 anchoring. We also evaluated the chemotaxis and transvascular migration of K237-PNEs using a transwell assay in the absence or presence of the human umbilical vein endothelial cells (HUVEC) monolayer, which utilized different percentages of tumor conditioned medium (TCM) to simulate the recruitment of inflammatory factors. As the proportion of TCM rose, the numbers of K237-PNEs transported to the lower chamber were gradually increased, but without significant variations with blank NEs (Fig. 3F and G, Supporting Information Fig. S11 and S12), implying that K237-PNEs remained the chemotaxis towards tumors and could proactively migrate across the vascular endothelium.

Besides, we further explored the stability of anchored K237 peptide on the surface of neutrophils, which plays essential roles in enhancing neutrophil extravasation. According to the TB quenching method, there were almost 84% K237 peptide (equivalent to 2.32 nmol per 10^6 cells) retained on the membrane within the first 4 h in the simulated chemotactic conditions (Fig. 3H), which suggested it could stay on the cell surface for recognition and binding with VEGFR2 in recruitment process due to its rapid response to inflammation and thereby laid a foundation for enhanced tumor-specific neutrophil extravasation. However, the amount of K237 peptide gradually reduced to 50% (equivalent to 1.40 nmol per 10^6 cells) after 8 h (Fig. 3H). The result indicated that the anchored K237 peptide would dislodge from the neutrophil membrane, which instead provided an opportunity for K237 peptide to block VEGFR2 on tumor vascular endothelial cells and inhibit the angiogenesis. Next, we further confirmed that the dislodged K237 peptide reserved the affinity to bind with endothelial cells, as verified by the fluorescence of K237 peptide distributed on HUVEC membrane despite partial K237 peptide located in cytoplasm (Fig. 3I). We also detected the variation of the amount of anchored K237 peptide during the trans-endothelial migration. Up to 27% of anchored K237 peptide was transferred to the membrane of HUVEC (Fig. 3J and Supporting Information Fig. S13), further indicating the potential function of anchored K237 peptide binding with vascular endothelial cells.

The stability of nab-PTX within K237-PNEs was also detected. We found that PTX kept stable in the cytoplasm except for a minor leakage in both normal and chemotactic conditions for 8 h (Supporting Information Fig. S14A and B), and only a small decline emerged when K237-PNEs crossed the HUVEC monolayer through the deformation movement (Supporting Information Fig. S14C).

In short, K237-PNEs could maintain the considerable stability for both membrane-anchored K237 and cytoplasm-internalized nab-PTX during the complex physiological process. And most crucially, anchored K237 peptide still possessed the affinity to bind with vascular endothelial cells, which might potentially exert the enhanced extravasation.

3.3. Accelerated tumor-specific extravasation and accumulation by K237-anchored neutrophil cytopharmaceuticals

Despite K237 peptide had been successfully anchored on the surface of PNEs, we wondered whether the anchored K237 peptide could accelerate the tumor accumulation and achieve the enhanced tumor-specific extravasation. We first confirmed the high expression of VEGFR2 on tumor blood vessles (Supporting Information Fig. S15) compared with normal mouse breast fat pad. Based on that, the in vivo biodistribution of K237-PNEs was evaluated with time on orthotopic triple-negative breast cancer (4 T1 cells)-bearing mice. The near-infrared probe DiR-labeled different neutrophil cytopharmaceuticals including fresh neutrophils (denote as NEs), PNEs and K237-PNEs were administrated and monitored using IVIS spectrum. Compared with the

unanchored NEs and PNEs, K237-PNEs showed an obviously higher DiR signal in tumor site within the first 12 h (Supporting Information Fig. S16), indicating more rapid tumor-targeting of K237-PNEs. Given the possible interference from the noticeable DiR signals in liver and spleen, tumor tissues were separately isolated and analyzed by region-of-interest (ROI, Fig. 4A and B). There were no significant differences between NEs and PNEs within 48 h, which confirmed that nab-PTX loading in the cytoplasm caused no adverse impact on the recruitment

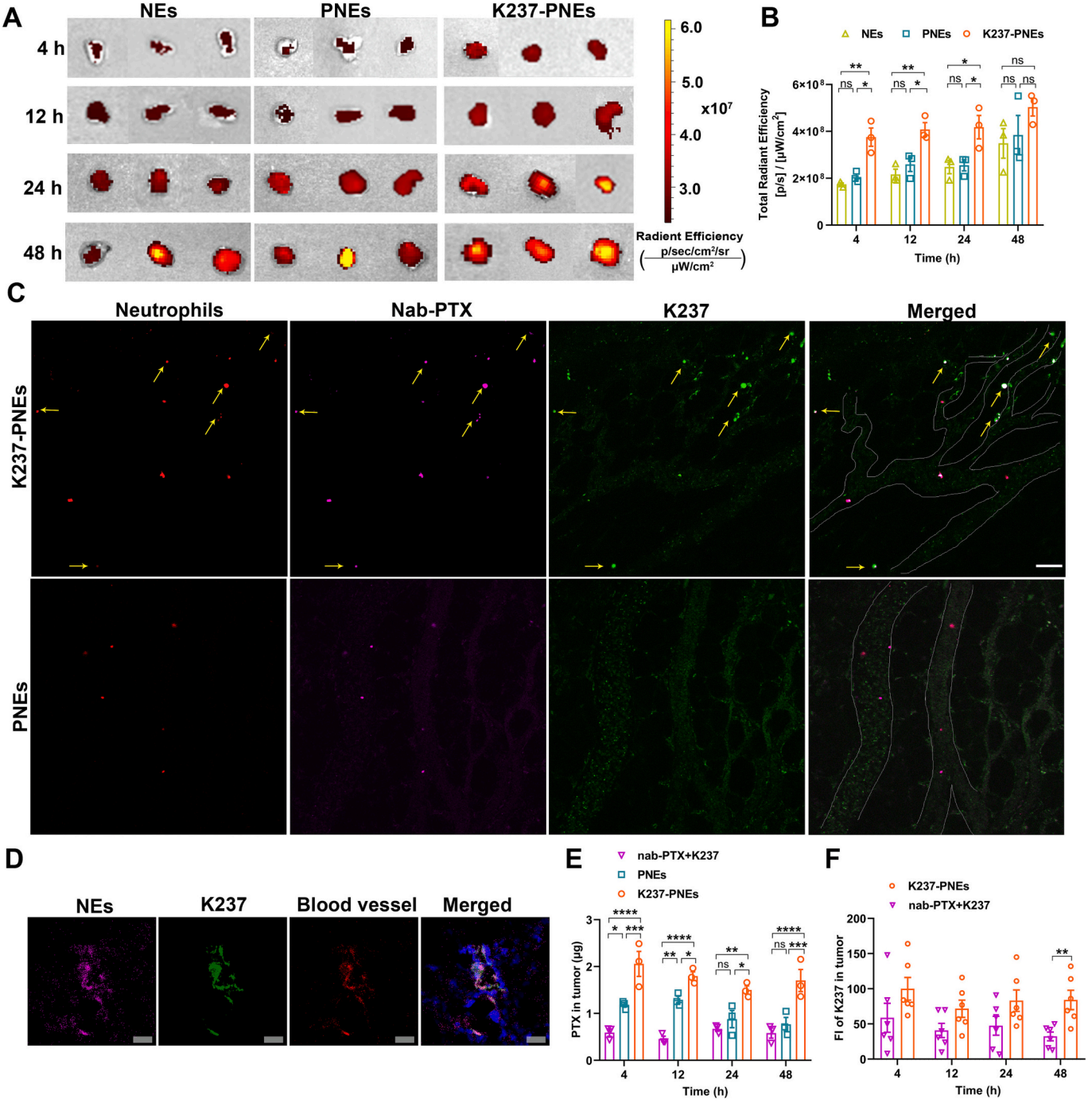

Fig. 4. Accelerated tumor-specific accumulation and extravasation by K237-PNEs. (A) The ex vivo imaging and (B) fluorescence quantification of tumor tissues isolated from the 4 T1 tumor-bearing mice after intravenous administration of DiR-labeled NEs, PNEs and K237-PNEs at a dosage of 2×10^7 cells each mouse over time ($n = 3$ mice per group). (C) The real-time intravital observation of neutrophils cytopharmaceuticals PNEs and K237-PNEs crossing the tumor blood vessels after 1 h of neutrophils infusion. Neutrophils, nab-PTX and K237 were respectively labeled by Cell Trace Far Red (red), Rhodamine B (magenta) and FITC (green). White dashed line indicated the border of blood vessels and the yellow arrows indicated the extravasated neutrophils from blood vessels. Scale bar = 50 μm. (D) The CLSM images of the frozen tumor tissue sections collected from the 4 T1 tumor-bearing mice after intravenous administration of K237-PNEs. NEs, K237 and tumor blood vessels were respectively labeled by DiR (magenta), FITC (green) and Alexa Fluor 594 anti-CD31 antibody (red). Scale bar = 20 μm. (E) Quantification of PTX in the tumor tissues from 4 T1-bearing mice (n = 3) after intravenous injection of different PTX formulations at a PTX dosage of 2.5 mg/kg over time. (F) The quantified fluorescence intensity of K237 in tumor tissues from 4 T1-bearing mice after intravenous administration of different K237 preparations at K237 dosage of 2.9 μmol/kg over time. All data are mean ± SEM. $^*P < 0.05$, $^{**}P < 0.01$ and $^{***}P < 0.001$. ns, not significant. (For interpretation of the references to colour in this figure legend, the reader is referred to the web version of this article.)

and migration of neutrophils. However, more K237-PNEs could accumulate into tumor as early as 4 h while PNEs and NEs showed a relative weaker and delayed tumor-infiltration until 48 h, which suggested that anchored K237 peptide could truly promote the tumor-targeting of neutrophil cytopharmaceuticals (Fig. 4A-B, Supporting Information Fig. S17). Notably, all neutrophils showed a initial accumulation in organs with abundant blood perfusion like liver, spleen and lung but decreased with time, which might account for the gradual increased neutrophils accumulation in tumor (Supporting Information Fig. S18).

Then we conducted the in vivo real-time observation of vascular extravasation for PNEs and K237-PNEs. We found that most of K237-PNEs extravasated from the vessel to infiltrate into the tumor tissue just after 1 h of injection, as marked with yellow arrows in Fig. 4C, while PNEs mainly stayed in the blood vessels in the short time. The process of crawling and extravasation of K237-PNEs could be clearly observed in the supplemented video of K237-PNEs, which was also illustrated through the intercepted representative images in Supporting Information Fig. S19. And most PNEs quickly migrated in the blood vessels and few PNEs adhered to blood vessels in the supplemented video of PNEs. These data indicated the accelerated extravasation capability of K237-PNEs due to the K237 anchoring. Besides, we noticed the weakened green fluorescence on some K237-PNEs inside blood vessels and after crossing the vessels, which can be ascribed to the lost of K237 peptide from neutrophils in the process of transvascular migration. This shortcoming in turn made K237 liable to stay on the vessel wall to block the VEGFR2 and perform the antiangiogenic effect, as confirmed by the observation that a large amount of green fluorescence on the vessel wall without the colocalization of neutrophils (red) and nab-PTX (magenta) (Fig. 4C and Supporting Information Fig. S19).

Synchronously, we conducted fluorescence observation of tumor tissue sections after injection of neutrophil cytopharmaceuticals for different time. Although PNEs and K237-PNEs could both migrate to the tumor vessels at 1 h, K237-PNEs arrived and started to extravasate from vessels at 2 h while PNEs delayed to 4 h (Supporting Information Fig. S20), which was probably due to the strengthened adhesion of neutrophils to tumor vessels through the binding effect of K237 and tumor vessels (Fig. 4D), thus accelarating the neutrophil extravasation into the tumor tissues.

Next, we quantitively detected the distribution of PTX and K237 peptide for evaluating the drug deposition brought by enhanced extravasation. In comparison with the mixture of free nab-PTX and K237 peptide (nab-PTX + K237) that showed limited PTX accumulation and quick elimination in tumor tissues, the gradual migration of PNEs to tumor site as time extended resulted in a significant higher PTX deposition witnin 12 h (Fig. 4E). However, the PTX amount decreased to almost the same level with free nab-PTX as time extended to 48 h owing to drug metabolism and clearance. By contrast, based on the expedited extravasation of K237-PNEs, significantly elevated PTX accumulation in tumor at 4 h was quantified, which was 4-folds and 2-folds higher than the drug mixture and PNEs respectively (Fig. 4E). Moreover, K237-PNEs could maintain a higher PTX amount up to 48 h in tumor site, which was still 3-folds and 2.2-folds higher than the drug mixture and PNEs respectively. These data verified that K237-PNEs accelerated the accumulation of loading drugs in solid tumor based on the enhanced tumor-specific extravasation. Despite the distribution of PNEs and K237-PNEs in normal organs, PNEs and K237-PNEs both showed higher tumor-targeting efficiency than free nab-PTX + K237 according to the PTX amount ratio after 48 h (Supporting Information Fig. S21 and S22). Notably, the gradual decreased amount of PTX in tumor tissues due to the PTX metabolism was inconsistent with the DiR signal of the neutrophil in IVIS spectrum, which might be owing to the slower metabolism and elimination of DiR especially in the cell-binding state (Fig. 4A and E). Similarly, K237-PNEs considerably increased the retention of K237 peptide in tumor tissue for at least 48 h and reduced the renal clearance (Fig. 4F and Supporting Information Fig. S23), meaning that K237-PNEs could significantly augment the collaborative efficacy of nab-PTX and K237 peptide on the basis of accelerated tumor accumulation and prolonged retention. In brief, we demonstrated that K237 anchoring has promoted tumor-specific extravasation of neutrophils in solid tumors, which had the potential to elicit enhanced anti-tumor effect due to the increased drug accumulation at tumor site.

3.4. The anti-angiogenesis and tumor killing effect of K237-PNEs in vitro

To further detect the bioactivity of K237-PNEs, the inhibition effect on the proliferation, migration and neovascularization of vascular endothelial cells were firstly explored. Free K237 or nab-PTX both showed strong inhibition on HUVEC proliferation and migration, which respectively derived from direct VEGFR blocking of K237 and the cytotoxicity of paclitaxel to HUVEC within 12–48 h. Compared to the free nab-PTX or K237 peptide, K237-PNEs performed a cooperative effect and evidently suppressed the proliferation of HUVEC with an increased inhibition ratio by 2.1- and 1.7-folds respectively (Fig. 5A). Similar inhibition could be found in the HUVEC migration by K237-PNEs, about 1.5-and 1.6-folds higher than free nab-PTX and K237, respectively (Fig. 5B). It's worth noting that because of the immediate interaction of nab-PTX + K237 on HUVEC without in vivo physiological barriers, K237-PNEs presented limited advantages over nab-PTX + K237 on both proliferation and migration of HUVEC in vitro. Besides, K237-PNEs showed a parallel inhibition activity in anti-angiogenesis evaluation with K237 and nab-PTX + K237 at 6 h, in which K237 peptide directly blocked the tube-formation of HUVEC and significantly decreased the branches points and branches length (Fig. 5C-E). This also confirmed the anchoring caused no intervention of anti-angiogenic function of K237. Despite nab-PTX inhibition on HUVEC proliferation and migration within 12–48 h in Fig. 5A-B, nab-PTX showed only slight suppression on angiogenesis in a short time of 6 h while PNEs exhibited almost no effect on angiogenesis because of almost no PTX release within 6 h (Fig. 5C-E, Supporting Information Fig. S14). Taken together, K237-PNEs retained the necessary capabilities of inhibiting the proliferation, migration, and neovascularization of vascular endothelial cells, which set up the foundation of the anti-angiogenesis therapy in concert with chemotherapy.

Next, the in vitro tumor-killing effect was detected against the luciferase-transfected 4 T1 cells (4 T1-luci). Although free nab-PTX or free K237 showed significant tumor-inhibition effect compared to the control, K237-PNEs exhibited a stronger cytotoxicity against the tumor cells than any of them (Fig. 5F), indicating a synergistic treatment strategy enhancing the anti-tumor effect. Given that K237-PNEs themselves released nab-PTX through the formation of NETs in the TCM stimulated tumor environment, as confirmed by CLSM (Supporting Information Fig. S24), the more aggravated tumor cytotoxicity than the nab-PTX + K237 group might result from the related tumor-killing cytokines of NETs [42–44].

In summary, these data verified that the anchored K237 peptide retained the capabilities of VEGFR targeting and anti-angiogenesis, as well as the synergistic anti-tumor effect with nab-PTX in vitro.

3.5. Boosted antitumor efficacy against orthotopic triple-negative breast cancer

The therapeutic effect of K237-PNEs was evaluated on the orthotopic triple-negative breast cancer-bearing mice according to the treatment regimen (Fig. 6A). In comparison to saline, blank NEs exhibited a relatively weak anti-tumor effect which herein mainly worked as the delivery vectors for nab-PTX and K237. Although free nab-PTX and free K237 have showed slight inhibiton in tumor growth like reduced tumor volume and tumor weight, the inhibition effect was almost no significant differences with the saline and markedly inferior to K237-PNEs (Fig. 6B-D). These results were further confirmed by the images of isolated tumor tissues (Supporting Information Fig. S25) and H&*E*-stained tumor sections (Fig. 6E). It's worth noting that combined administration of free

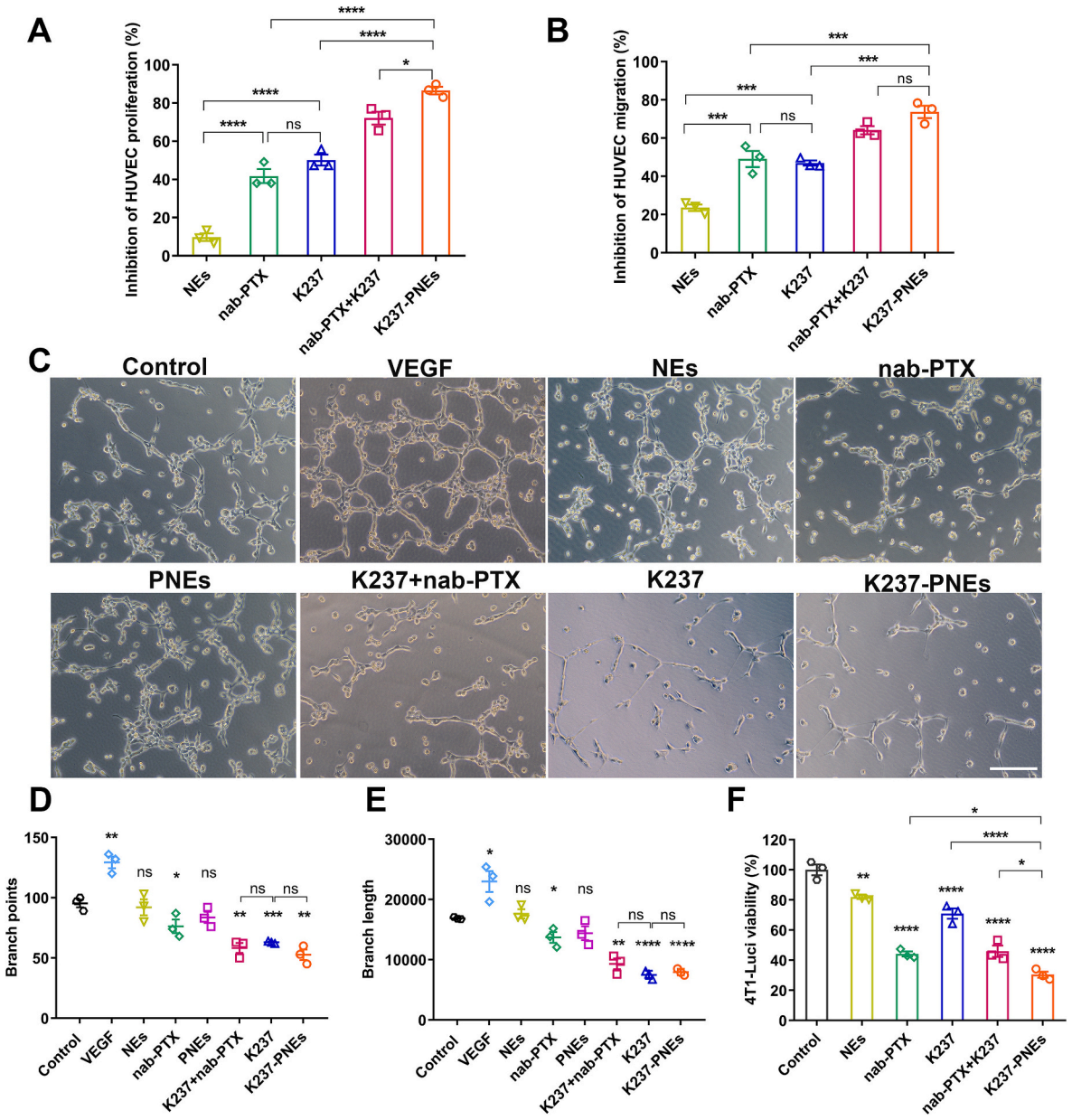

Fig. 5. The anti-angiogenic and tumor-killing effect in vitro. (A) Inhibition rate of HUVEC proliferation mediated by K237-PNEs compared with other formulations. (B) Inhibition rate of HUVEC migration using the transwell assay affected by K237-PNEs compared with other formulations. (C) The inhibition on neovascularization networks by K237-PNEs. Scale bar = 100 μm. The quantitative results on the branch points (D) and branch length (E) of the neovascularization were analyzed from random three fields by image J. (F) Cytotoxicity against 4 T1-Luci cells using firefly luciferase reporter gene. All data are mean ± SEM ($n = 3$). * $P < 0.05$, ** $P < 0.01$, *** $P < 0.001$ and **** $P < 0.0001$. ns, not significant.

K237 and PNEs (K237 + PNEs) could truly generate improved therapeutic efficacy because of the synergistic effects of cytotoxicity and antiangiogenesis, however, K237-PNEs exerted around 1.4-folds higher tumor-inhibition than K237 + PNEs (Fig. 6D), and remarkedly shrunk the tumor size. The considerably enhanced therapeutic effect of K237-PNEs could be attributed to the elevated tumor-accumulation and decreased blood-clearance of K237 peptide, thus achieving maximized cooperation of these two drugs based on the enhanced tumor-specific extravasation. Meanwhile, K237-PNEs also showed obvious inhibition of tumor angiogenesis than free K237 or K237 + PNEs, as confirmed by vascular immunofluorescence of tumor tissue sections (Fig. 6F and G). Additionally, K237 + PNEs showed no significant differences with free K237 (Fig. 6F and G), further implying that anchored K237 on PNEs vastly improved the accumulation in tumor sites and maximally exert the anti-proliferation and anti-angiogenesis effect. As a result, K237-PNEs obviously prolonged the survival based on the lessened neovascularization and shrunken tumor size than other groups (Fig. 6H). The median survival time of K237-PNEs extended about 1.2- and 1.3-folds longer than that of K237 + PNEs and free nab-PTX groups, respectively (Fig. 6H). These data manifested that a synergistic inhibition of tumor growth and angiogenesis could be achieved by K237-anchored neutrophil cytopharmaceuticals, thus boosting the therapeutic efficacy in solid tumors.

Moreover, the safety of K237-PNEs was also evaluated. The body weights and the main organ indexes (Fig. 6I and J) of mice receiving different treatment showed no substantial differences between K237-PNEs and the other groups. No pathological changes were observed from the H&*E*-staining images of the main organ sections (Supporting Information Fig. S26), and the functions of liver and kidney in terms of alanine aminotransferase (ALT), aspartate aminotransferase (AST),

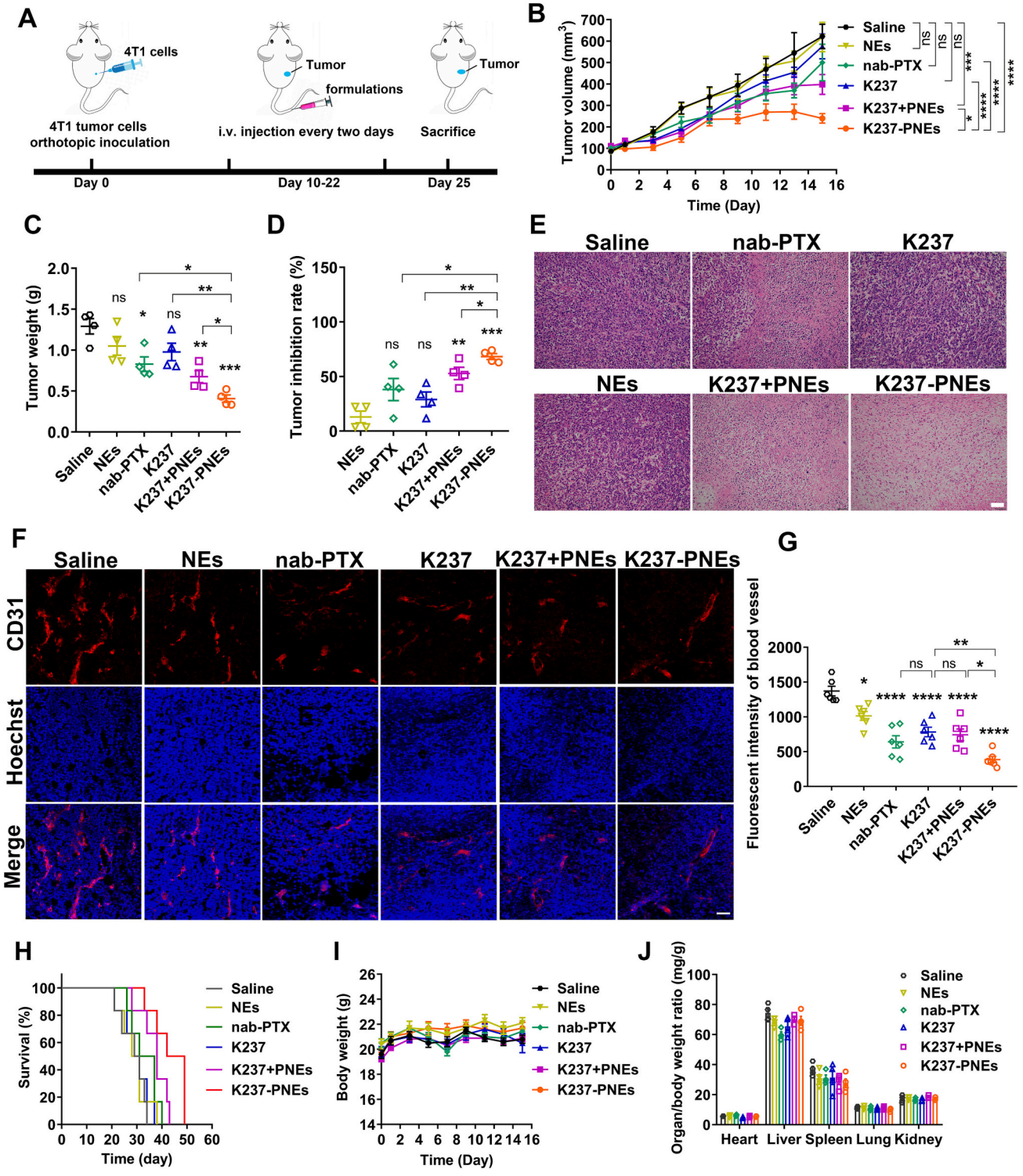

Fig. 6. Evaluation of the anti-tumor effect and safety of K237-PNEs in orthotopic 4 T1 tumor-bearing mice. (A) Schematic illustration of the administration regimen. (B) The tumor growth curves, (C) tumor weight and (D) the tumor-inhibition rate after treatment of different formulations including saline, nab-PTX (2.5 mg/kg), K237 (2.9 μmol/kg), NEs (1×10^9 cells/kg), K237 + PNEs (2.9 μmol/kg K237, 1×10^9 cells/kg PNEs equivalent to 2.5 mg/kg PTX), K237-PNEs (1×10^9 cells/kg, equivalent to 2.5 mg/kg PTX and 2.9 μmol/kg K237) from Day 10. Data are mean ± SEM, $n = 4$ mice per group. (E) Histological images of the H&E-stained tumor sections collected from the mice treated with saline, nab-PTX, K237, NEs, K237 + PNEs and K237-PNEs. Scale bar = 100 μm. (F) The frozen tumor tissue sections labeled by Alexa Fluor 594 anti-CD31 antibody after different treatment were observed by CSLM. Scale bar = 50 μm. (G) The quantitative fluorescence intensity of tumor vessels from frozen tissue sections of 4 T1 tumor-bearing mice after different treatment. The vascular abundance was analyzed from six random frozen tissue sections of each group by Image J. Data are mean ± SEM ($n = 6$). (H) Survival curves of 4 T1 tumor-bearing mice (6 mice per group) after intravenous administration of different formulations. (I) The changes in body weights of 4 T1 tumor-bearing mice after treatment over time. Data are mean ± SEM, n = 4 mice per group. (J) The main organ index of the 4 T1-bearing mice after treatment with different formulations. Data are mean ± SEM, n = 4 mice per group. *$P < 0.05$, ** $P < 0.01$, *** $P < 0.001$ and **** $P < 0.0001$. ns, not significant.

alkaline phosphatase (ALP), lactate dehydrogenase (LDH) and blood urea nitrogen (BUN) for K237-PNEs were all within the normal range (Supporting Information Fig. S27). Further, the number of leukocytes, erythrocytes, and platelets as well as the amount of hemoglobin displayed no evident variation (Supporting Information Fig. S28).

Taken together, we demonstrated that K237-PNEs achieved the boosted anticancer efficacy via the effective anti-angiogenesis, improved inhibition of tumor growth, and prolonged survival, which attributed to the enhanced tumor-specific extravasation and thus the extended accumulation of K237 peptide and PTX in tumor site.

4. Discussion

Chronic inflammation is a hallmark of cancer and exerts pleiotropic effects in the development of cancer, including favoring carcinogenesis, tumor growth and even aggravating invasion and metastasis [45–47]. During the progression, diverse immune cells, such as neutrophils, macrophages, lymphocytes, monocytes and et al. are recruited and infiltrate to the precancerous lesions to exert either pro- or anti-tumor effects and affect therapeutic resistance [48–50]. It has been reported that neutrophils exhibit a higher infiltration proportion than the other immunocytes in various solid tumors probably owing to the most abundant quantity and first-line defense when inflammation occurs, which lays a foundation for neutrophil cytopharmaceuticals to be exploited for promoting the drug accumulation at tumor site [51]. Based on the chemotaxis to inflammatory cytokines of neutrophils, we have explored the adjuvant treatment such as surgery, radiotherapy or photothermal therapy to amplify the inflammation levels in local tumor sites, in which rapid migration of neutrophil cytopharmaceuticals to the tumor within 2 h have been demonstrated even facing the blood-brain barrier. Moreover, based on the chemotaxis to some specific cytokines derived from TME such as lung metastases, the substantial suppression effect of neutrophil cytopharmaceuticals has also been revealed. However, it can't be ignored that neutrophils themselves tend to colonize in the organs with abundant blood perfusion and immunological competence such as the lung [52,53]. The chronic inflamed level and disordered vasculature in solid tumor tissue presents a great challenge for quick and specific extravasation of neutrophils. Inspired by the physiological mechanism of neutrophil extravasation and the typical feature of VEGFR highly expressing on tumor vasculature, we proposed an enhanced tumor-specific extravasation strategy via anchoring the VEGFR2-targeted peptide K237 on neutrophil membrane, thus promoting the accumulation of neutrophil cytopharmaceuticals in tumor sites and eliciting the combined anti-angiogenesis and tumor-killing effect.

Currently, only several mechanisms have indicated the potential of improving the neutrophil chemotaxis to inflammation. For instance, activated platelets can reinforce neutrophil recruitment through enhanced interaction with neutrophils through surface high-expressed P-selectin, released soluble chemokines (CCL5), as well as the latest reported inflammation mediator 5-HIAA that cam bind with the receptor GPR35 on activated neutrophils [54]. In addition, Dipeptidase 1 membrane protein on endothelium as a physical adhesion receptor can facilitate neutrophils to inflamed sites in lung and liver [55]. However, great challenges remain in transforming these physiological mechanisms to applications, especially in the context of tissue-specific recruitment modes [27,56]. In this work, we leveraged the VEGFR2 as a universal tumor-specific "landmark", which highly expressed on neovascular endothelial cells in nearly all of solid tumors. The anchored VEGFR2-targeting peptide on the neutrophil surface can specifically recognize the tumor site and provides an extra tether for neutrophil cytopharmaceuticals to bind to and adherent with the vessel wall, which elicits the following deformation and extravasation. Moreover, the anchored VEGFR2-targeting peptide also serves as the anti-angiogenesis agents to inhibit the formation of neovascular, which achieves a combined therapeutic efficacy with cytotoxic drugs.

Given that the role of K237 peptides required to be located outside the cell to interact with vascular endothelial cells and promote neutrophils extravasation, we changed the traditional drug-loading method into anchoring K237 on cell membrane using a membrane-anchoring technic. Further, we modified the drug-loading process by anchoring K237 peptide after phagocytic loading of chemotherapeutics. We demonstrated this improved method reduced the cellular endocytosis of K237, meanwhile showed no adverse effect on the physiological functions of neutrophils. Moreover, the modest cell membrane-anchoring provides either the stable anchoring of VEGFR2-targeting peptide during the chemotaxis process or the available dislodging of VEGFR2-targeting peptide for anti-angiogenesis during the extravasation process. Most importantly, the membrane-anchored K237 exhibited two critical functions that complemented each other, which could not only enhance neutrophils extravasation but also further exerted synergistic anti-tumor effect with chemotherapeutics. Based on the improved accumulation and retention of VEGFR2-targeting peptide and PTX, the peptide-anchored neutrophil cytopharmaceuticals held the strongest inhibition on tumor growth and thus prolonged the survival.

In view of clinical treatment of triple-negative breast cancer, using nab-PTX is inevitable to face the challenge of unsatisfied targeting-efficiency and lower drug deposition in tumor. The neutrophils cytopharmaceuticals PNEs herein significantly increased the tumor-targeting of nab-PTX based on the neutrophils proactive tumor-tropism. Most importantly, K237-PNEs further expedited the neutrophils migration and tumor-extravasation, achieving further enhanced drug accumulation and anti-tumor effect. Briefly, we completed the preliminary proof of concept about the great therapeutic advantages and potential clinical value for K237-PNEs. This inspired us to explore the therapy effect in other malignant tumors and advance the clinical application in future.

5. Conclusion

In summary, we have proposed a new generation of neutrophil cytopharmaceuticals with enhanced tumor-specific extravasation by peptide anchoring, which also exhibited improved antitumor effect through the combined anti-angiogenesis and cytotoxicity. Our evolutionary drug-loading technic based on the traditional endocytic method provides a larger platform for collaborative delivery of drugs with different properties, in parallel, indicates a promising direction for cytopharmaceuticals or even living cells in enhanced extravasation to targeted sites in more therapeutic application.

Supplementary data to this article can be found online at https://doi.org/10.1016/j.jconrel.2023.05.037.

Author contributions

Luping Zhang designed and conducted all experiments, analyzed the data, wrote and revised the manuscript. Qianqian Wang conducted all experiments, analyzed the data, and wrote the original manuscript. Yupeng Dai assisted in cell experiments. Jiaqi Chen and Tong Wu assisted in mice experiments. Caoyun Ju supervised most of experiments and assisted in revising the manuscript. Lingjing Xue conceived the project. Can Zhang conceived the project, supervised all experiments, and assisted in revising the manuscript. All of the authors have read and approved the final manuscript.

CRediT authorship contribution statement

Luping Zhang: Writing – review & editing, Writing – original draft, Visualization, Validation, Software, Methodology, Investigation, Formal analysis, Data curation, Conceptualization. **Qianqian Wang:** Writing – original draft, Validation, Methodology, Investigation, Formal analysis, Conceptualization. **Yupeng Dai:** Methodology, Investigation. **Jiaqi Chen:** Investigation. **Tong Wu:** Investigation. **Caoyun Ju:** Supervision,

Conceptualization, Writing - review & editing. **Lingjing Xue:** Supervision, Project administration, Conceptualization. **Can Zhang:** Writing – review & editing, Supervision, Resources, Project administration, Funding acquisition, Conceptualization.

Declaration of Competing Interest

The authors declare no competing interests.

Data availability

Data will be made available on request.

Acknowledgements

This work was supported by the National Natural Science Foundation of China (81930099, 82130102, 92159304, 82003694), the Natural Science Foundation of Jiangsu Province (BK20212011, China), Technology innovation project of Nucleic acid drug from National Center of Technology Innovation for Biopharmaceuticals (NCTIB2022HS01014), National Major Scientific and Technological Special Project for "Significant New Drugs Development" (2019ZX09301163), "Double First-Class" University project (CPU2022QZ05, China), 111 Project from the Ministry of Education of China and the State Administration of Foreign Expert Affairs of China (No. 111-2-07, B17047), and the Project Program of State Key Laboratory of Natural Medicines (China Pharmaceutical University, No. SKLNMZZ202223). The authors thank Jiangsu Key Laboratory of Drug Design and Optimization for assistance with the molecule design and optimization.

References

[1] D.J. Hicklin, L.M. Ellis, Role of the vascular endothelial growth factor pathway in tumor growth and angiogenesis, J. Clin. Oncol. 23 (2005) 1011–1027, https://doi.org/10.1200/JCO.2005.06.081.
[2] C.H. Heldin, K. Rubin, K. Pietras, A. Ostman, High interstitial fluid pressure - an obstacle in cancer therapy, Nat. Rev. Cancer 4 (2004) 806–813, https://doi.org/10.1038/nrc1456.
[3] W. Zou, Immunosuppressive networks in the tumour environment and their therapeutic relevance, Nat. Rev. Cancer 5 (2005) 263–274, https://doi.org/10.1038/nrc1586.
[4] R.K. Jain, Vascular and interstitial barriers to delivery of therapeutic agents in tumors, Cancer Metastasis Rev. 9 (1990) 253–266, https://doi.org/10.1007/BF00046364.
[5] J. Fang, H. Nakamura, H. Maeda, The EPR effect: unique features of tumor blood vessels for drug delivery, factors involved, and limitations and augmentation of the effect, Adv. Drug Deliv. Rev. 63 (2011) 136–151, https://doi.org/10.1016/j.addr.2010.04.009.
[6] M.K. Danquah, X.A. Zhang, R.I. Mahato, Extravasation of polymeric nanomedicines across tumor vasculature, Adv. Drug Deliv. Rev. 63 (2011) 623–639, https://doi.org/10.1016/j.addr.2010.11.005.
[7] Y. Nakamura, A. Mochida, P.L. Choyke, H. Kobayashi, Nanodrug delivery: is the enhanced permeability and retention effect sufficient for curing Cancer? Bioconjug. Chem. 27 (2016) 2225–2238, https://doi.org/10.1021/acs.bioconjchem.6b00437.
[8] H. Kang, S. Rho, W.R. Stiles, S. Hu, Y. Baek, D.W. Hwang, S. Kashiwagi, M.S. Kim, H.S. Choi, Size-dependent EPR effect of polymeric nanoparticles on tumor targeting, Adv. Healthc. Mater. 9 (2020), e1901223, https://doi.org/10.1002/adhm.201901223.
[9] H. Wang, Z. Feng, B. Xu, Bioinspired assembly of small molecules in cell milieu, Chem. Soc. Rev. 46 (2017) 2421–2436, https://doi.org/10.1039/c6cs00656f.
[10] Y. Cong, L. Ji, Y.J. Gao, F.H. Liu, D.B. Cheng, Z. Hu, Z.Y. Qiao, H. Wang, Microenvironment-induced in situ self-assembly of polymer-peptide conjugates that attack solid tumors deeply, Angew. Chem. Int. Ed. 58 (2019) 4632–4637, https://doi.org/10.1002/anie.201900135.
[11] K. Wang, X. Zhang, Y. Liu, C. Liu, B. Jiang, Y. Jiang, Tumor penetrability and anti-angiogenesis using iRGD-mediated delivery of doxorubicin-polymer conjugates, Biomaterials 35 (2014) 8735–8747, https://doi.org/10.1016/j.biomaterials.2014.06.042.
[12] Y. Jiang, X. Pang, R. Liu, Q. Xiao, P. Wang, A.W. Leung, Y. Luan, C. Xu, Design of an amphiphilic iRGD peptide and self-assembling nanovesicles for improving tumor accumulation and penetration and the photodynamic efficacy of the photosensitizer, ACS Appl. Mater. 10 (2018) 31674–31685, https://doi.org/10.1021/acsami.8b11699.
[13] L. Li, T.L. ten Hagen, M. Bolkestein, A. Gasselhuber, J. Yatvin, G.C. van Rhoon, A. M. Eggermont, D. Haemmerich, G.A. Koning, Improved intratumoral nanoparticle extravasation and penetration by mild hyperthermia, J. Control. Release 167 (2013) 130–137, https://doi.org/10.1016/j.jconrel.2013.01.026.
[14] M. Zhang, S. Gao, D. Yang, Y. Fang, X. Lin, X. Jin, Y. Liu, X. Liu, K. Su, K. Shi, Influencing factors and strategies of enhancing nanoparticles into tumors in vivo, Acta Pharm. Sin. B 11 (2021) 2265–2285, https://doi.org/10.1016/j.apsb.2021.03.033.
[15] Y. Shi, R. van der Meel, X. Chen, T. Lammers, The EPR effect and beyond: strategies to improve tumor targeting and cancer nanomedicine treatment efficacy, Theranostics 10 (2020) 7921–7924, https://doi.org/10.7150/thno.49577.
[16] S. Sindhwani, A.M. Syed, J. Ngai, B.R. Kingston, L. Maiorino, J. Rothschild, P. MacMillan, Y. Zhang, N.U. Rajesh, T. Hoang, J.L.Y. Wu, S. Wilhelm, A. Zilman, S. Gadde, A. Sulaiman, B. Ouyang, Z. Lin, L. Wang, M. Egeblad, W.C.W. Chan, The entry of nanoparticles into solid tumours, Nat. Mater. 19 (2020) 566–575, https://doi.org/10.1038/s41563-019-0566-2.
[17] R.M. Bremnes, K. Al-Shibli, T. Donnem, R. Sirera, S. Al-Saad, S. Andersen, H. Stenvold, C. Camps, L.T. Busund, The role of tumor-infiltrating immune cells and chronic inflammation at the tumor site on cancer development, progression, and prognosis: emphasis on non-small cell lung cancer, J. Thorac. Oncol. 6 (2011) 824–833, https://doi.org/10.1097/JTO.0b013e3182037b76.
[18] K. Ley, H.M. Hoffman, P. Kubes, M.A. Cassatella, A. Zychlinsky, C.C. Hedrick, S. D. Catz, Neutrophils: New insights and open questions, Sci. Immunol. 3 (2018), eaat4579, https://doi.org/10.1126/sciimmunol.aat4579.
[19] K.A. Schalper, M. Carleton, M. Zhou, T. Chen, Y. Feng, S.P. Huang, A.M. Walsh, V. Baxi, D. Pandya, T. Baradet, D. Locke, Q.Y. Wu, T.P. Reilly, P. Phillips, V. Nagineni, N. Gianino, J.L. Gu, H.Y. Zhao, J.L. Perez-Gracia, M.F. Sanmamed, I. Melero, Elevated serum interleukin-8 is associated with enhanced intratumor neutrophils and reduced clinical benefit of immune-checkpoint inhibitors, Nat. Med. 26 (2020) 688–692, https://doi.org/10.1038/s41591-020-0856-x.
[20] S.K. Wculek, I. Malanchi, Neutrophils support lung colonization of metastasis-initiating breast cancer cells, Nature 528 (2015) 413–417, https://doi.org/10.1038/nature16140.
[21] S.B. Coffelt, K. Kersten, C.W. Doornebal, J. Weiden, K. Vrijland, C.S. Hau, N.J. M. Verstegen, M. Ciampricotti, L.J.A.C. Hawinkels, J. Jonkers, K.E. de Visser, IL-17-producing gamma delta T cells and neutrophils conspire to promote breast cancer metastasis, Nature 522 (2015) 345–348, https://doi.org/10.1038/nature14282.
[22] S.B. Coffelt, M.D. Wellenstein, K.E. de Visser, Neutrophils in cancer: neutral no more, Nat. Rev. Cancer 16 (2016) 431–446, https://doi.org/10.1038/nrc.2016.52.
[23] E. Kolaczkowska, P. Kubes, Neutrophil recruitment and function in health and inflammation, Nat. Rev. Immunol. 13 (2013) 159–175, https://doi.org/10.1038/nri3399.
[24] J. Xue, Z. Zhao, L. Zhang, L. Xue, S. Shen, Y. Wen, Z. Wei, L. Wang, L. Kong, H. Sun, Q. Ping, R. Mo, C. Zhang, Neutrophil-mediated anticancer drug delivery for suppression of postoperative malignant glioma recurrence, Nat. Nanotechnol. 12 (2017) 692–700, https://doi.org/10.1038/nnano.2017.54.
[25] C. Ju, Y. Wen, L. Zhang, Q. Wang, L. Xue, J. Shen, C. Zhang, Neoadjuvant chemotherapy based on Abraxane/human neutrophils cytopharmaceuticals with radiotherapy for gastric cancer, Small 15 (2019), e1804191, https://doi.org/10.1002/smll.201804191.
[26] L. Zhang, Y. Zhang, Y. Xue, Y. Wu, Q. Wang, L. Xue, Z. Su, C. Zhang, Transforming weakness into strength: Photothermal-therapy-induced inflammation enhanced cytopharmaceutical chemotherapy as a combination anticancer treatment, Adv. Mater. 31 (2019), e1805936, https://doi.org/10.1002/adma.201805936.
[27] A. Margraf, K. Ley, A. Zarbock, Neutrophil recruitment: from model systems to tissue-specific patterns, Trends Immunol. 40 (2019) 613–634, https://doi.org/10.1016/j.it.2019.04.010.
[28] Y. Li, Q. Hu, W. Li, S. Liu, K. Li, X. Li, J. Du, Z. Yu, C. Wang, C. Zhang, Simultaneous blockage of contextual TGF-beta by cyto-pharmaceuticals to suppress breast cancer metastasis, J. Control. Release 336 (2021) 40–53, https://doi.org/10.1016/j.jconrel.2021.06.012.
[29] J. Du, C. Wang, Y. Chen, L. Zhong, X. Liu, L. Xue, Y. Zhang, Y. Li, X. Li, C. Tang, Z. Su, C. Zhang, Targeted downregulation of HIF-1α for restraining circulating tumor microemboli mediated metastasis, J. Control. Release 343 (2022) 457–468, https://doi.org/10.1016/j.jconrel.2022.01.051.
[30] Y. Zhang, C. Wang, W. Li, W. Tian, C. Tang, L. Xue, Z. Lin, G. Liu, D. Liu, Y. Zhou, Q. Wang, X. Wang, L. Birnbaumer, Y. Yang, X. Li, C. Ju, C. Zhang, Neutrophil CYTO-pharmaceuticals suppressing tumor metastasis via inhibiting hypoxia-inducible factor-1α in circulating breast cancer cells, Adv. Healthc. Mater. 11 (2022), e2101761, https://doi.org/10.1002/adhm.202101761.
[31] M. De Palma, D. Biziato, T.V. Petrova, Microenvironmental regulation of tumour angiogenesis, Nat. Rev. Cancer 17 (2017) 457–474, https://doi.org/10.1038/nrc.2017.51.
[32] N.R. Smith, D. Baker, N.H. James, K. Ratcliffe, M. Jenkins, S.E. Ashton, G. Sproat, R. Swann, N. Gray, A. Ryan, J.M. Jürgensmeier, C. Womack, Vascular endothelial growth factor receptors VEGFR-2 and VEGFR-3 are localized primarily to the vasculature in human primary solid cancers, Clin. Cancer Res. 16 (2010) 3548–3561, https://doi.org/10.1158/1078-0432.CCR-09-2797.
[33] V. Thakur, R.V. Kutty, Recent advances in nanotheranostics for triple negative breast cancer treatment, J. Exp. Clin. Cancer Res. 38 (2019) 430–452, https://doi.org/10.1186/s13046-019-1443-1.
[34] J.V. Vermaas, E. Tajkhorshid, A microscopic view of phospholipid insertion into biological membranes, J. Phys. Chem. B 118 (2014) 1754–1764, https://doi.org/10.1021/jp409854w.
[35] E. Seyyednia, F. Oroojalian, B. Baradaran, J.S. Mojarrad, A. Mokhtarzadeh, H. Valizadeh, Nanoparticles modified with vasculature-homing peptides for

targeted cancer therapy and angiogenesis imaging, J. Control. Release 338 (2021) 367–393, https://doi.org/10.1016/j.jconrel.2021.08.044.
[36] D.H. Yu, Q. Lu, J. Xie, C. Fang, H.Z. Chen, Peptide-conjugated biodegradable nanoparticles as a carrier to target paclitaxel to tumor neovasculature, Biomaterials 31 (2010) 2278–2292, https://doi.org/10.1016/j.biomaterials.2009.11.047.
[37] J. Yao, J. Feng, X. Gao, D. Wei, T. Kang, Q. Zhu, T. Jiang, X. Wei, J. Chen, Neovasculature and circulating tumor cells dual-targeting nanoparticles for the treatment of the highly-invasive breast cancer, Biomaterials 113 (2017) 1–17, https://doi.org/10.1016/j.biomaterials.2016.10.033.
[38] M. Hao, S. Hou, W. Li, K. Li, L. Xue, Q. Hu, L. Zhu, Y. Chen, H. Sun, C. Ju, C. Zhang, Combination of metabolic intervention and T cell therapy enhances solid tumor immunotherapy, Sci. Transl. Med. 12 (2020), eaaz6667, https://doi.org/10.1126/scitranslmed.aaz6667.
[39] J.D. Loike, S.C. Silverstein, A fluorescence quenching technique using trypan blue to differentiate between attached and ingested glutaraldehyde-fixed red blood cells in phagocytosing murine macrophages, J. Immunol. Methods 57 (1983) 373–379, https://doi.org/10.1016/0022-1759(83)90097-2.
[40] S. Busetto, E. Trevisan, P. Patriarca, R. Menegazzi, A single-step, sensitive flow cytofluorometric assay for the simultaneous assessment of membrane-bound and ingested Candida albicans in phagocytosing neutrophils, Cytometry A 58 (2004) 201–206, https://doi.org/10.1002/cyto.a.20014.
[41] V.M. Steffes, Z. Zhang, S. MacDonald, J. Crowe, K.K. Ewert, B. Carragher, C. S. Potter, C.R. Safinya, PEGylation of paclitaxel-loaded cationic liposomes drives steric stabilization of bicelles and vesicles thereby enhancing delivery and cytotoxicity to human cancer cells, ACS Appl. Mater. Interfaces 12 (2020) 151–162, https://doi.org/10.1021/acsami.9b16150.
[42] V. Papayannopoulos, K.D. Metzler, A. Hakkim, A. Zychlinsky, Neutrophil elastase and myeloperoxidase regulate the formation of neutrophil extracellular traps, J. Cell Biol. 191 (2010) 677–691, https://doi.org/10.1083/jcb.201006052.
[43] A. Hidalgo, P. Libby, O. Soehnlein, I.V. Aramburu, V. Papayannopoulos, C. Silvestre-Roig, Neutrophil extracellular traps: from physiology to pathology, Cardiovasc. Res. (2021), https://doi.org/10.1093/cvr/cvab329.
[44] V. Papayannopoulos, Neutrophil extracellular traps in immunity and disease, Nat. Rev. Immunol. 18 (2018) 134–147, https://doi.org/10.1038/nri.2017.105.
[45] G. Multhoff, M. Molls, J. Radons, Chronic inflammation in cancer development, Front. Immunol. 2 (2012) 98–115, https://doi.org/10.3389/fimmu.2011.00098.
[46] E. Elinav, R. Nowarski, C.A. Thaiss, B. Hu, C. Jin, R.A. Flavell, Inflammation-induced cancer: crosstalk between tumours, immune cells and microorganisms, Nat. Rev. Cancer 13 (2013) 759–771, https://doi.org/10.1038/nrc3611.
[47] F.R. Greten, S.I. Grivennikov, Inflammation and cancer: triggers, mechanisms, and consequences, Immunity 51 (2019) 27–41, https://doi.org/10.1016/j.immuni.2019.06.025.
[48] L.M. Coussens, L. Zitvogel, A.K. Palucka, Neutralizing tumor-promoting chronic inflammation: a magic bullet? Science 339 (2013) 286–291, https://doi.org/10.1126/science.1232227.
[49] G. Bindea, B. Mlecnik, M. Tosolini, A. Kirilovsky, M. Waldner, A.C. Obenauf, H. Angell, T. Fredriksen, L. Lafontaine, A. Berger, P. Bruneval, W.H. Fridman, C. Becker, F. Pagès, M.R. Speicher, Z. Trajanoski, J. Galon, Spatiotemporal dynamics of intratumoral immune cells reveal the immune landscape in human cancer, Immunity 39 (2013) 782–795, https://doi.org/10.1016/j.immuni.2013.10.003.
[50] W.H. Fridman, F. Pagès, C. Sautès-Fridman, J. Galon, The immune contexture in human tumours: impact on clinical outcome, Nat. Rev. Cancer 12 (2012) 298–306, https://doi.org/10.1038/nrc3245.
[51] B.M. Allen, K.J. Hiam, C.E. Burnett, A. Venida, R. DeBarge, I. Tenvooren, D. M. Marquez, N.W. Cho, Y. Carmi, M.H. Spitzer, Systemic dysfunction and plasticity of the immune macroenvironment in cancer models, Nat. Med. 26 (2020) 1125–1134, https://doi.org/10.1038/s41591-020-0892-6.
[52] Z.M. Zhao, A. Ukidve, V. Krishnan, A. Fehnel, D.C. Pan, Y.S. Gao, J. Kim, M. A. Evans, A. Mandal, J.L. Guo, V.R. Muzykantov, S. Mitragotri, Systemic tumour suppression via the preferential accumulation of erythrocyte-anchored chemokine-encapsulating nanoparticles in lung metastases, Nat. Biomed. Eng. 5 (2021) 441–454, https://doi.org/10.1038/s41551-020-00644-2.
[53] N.K. Altorki, G.J. Markowitz, D. Gao, J.L. Port, A. Saxena, B. Stiles, T. McGraw, V. Mittal, The lung microenvironment: an important regulator of tumour growth and metastasis, Nat. Rev. Cancer 19 (2019) 9–31, https://doi.org/10.1038/s41568-018-0081-9.
[54] M. De Giovanni, H. Tam, C. Valet, Y. Xu, M.R. Looney, J.G. Cyster, GPR35 promotes neutrophil recruitment in response to serotonin metabolite 5-HIAA, Cell 185 (2022) 815–830, e819, https://doi.org/10.1016/j.cell.2022.01.010.
[55] S.R. Choudhury, L. Babes, J.J. Rahn, B.Y. Ahn, K.R. Goring, J.C. King, A. Lau, B. Petri, X. Hao, A.K. Chojnacki, A. Thanabalasuriar, E.F. McAvoy, S. Tabaries, C. Schraeder, K.D. Patel, P.M. Siegel, K.A. Kopciuk, D.C. Schriemer, D.A. Muruve, M.M. Kelly, B.G. Yipp, P. Kubes, S.M. Robbins, D.L. Senger, Dipeptidase-1 is an adhesion receptor for neutrophil recruitment in lungs and liver, Cell 178 (2019) 1205–1221, e1217, https://doi.org/10.1016/j.cell.2019.07.017. e1217.
[56] S. SenGupta, L.E. Hein, C.A. Parent, The recruitment of neutrophils to the tumor microenvironment is regulated by multiple mediators, Front. Immunol. 12 (2021), 734188, https://doi.org/10.3389/fimmu.2021.734188.